A Finite Element Study on the Impact of Arterial Plaque Composition on its Biomechanical Stability

by

Sephalie Y. Patel

B.S., Mechanical Engineering (2001)

Cornell University

Submitted to the Department of Mechanical Engineering in
Partial Fulfillment of the Requirements for the Degree of
Master of Science in Mechanical Engineering

at the

Massachusetts Institute of Technology

June 2003

Signature of Author.....
Department of Mechanical Engineering
May 9, 2003

Certified by.....
Roger D. Kamm
Professor of Mechanical Engineering and Bioengineering
Thesis Supervisor

Accepted by.....
Ain A. Sonin
Chairman, Department Committee on Graduate Students

A Finite Element Study on the Impact of Arterial Plaque Composition on its Biomechanical Stability

by

Sephalie Y. Patel

Submitted to the Department of Mechanical Engineering on May 9, 2003 in Partial Fulfillment of the Requirements for the Degree of Master of Science in Mechanical Engineering

ABSTRACT

Increased mechanical stresses in the arterial wall can lead to rupture of the fibrous cap, which encloses the arterial plaque, causing stroke or heart attack. By investigating the correlation between plaque composition and patterns of mechanical stress or strain, we aim to provide mechanical markers to foresee the vulnerability of plaque for rupture. Specimens excised during surgical removal of an obstruction in the carotid artery (endarterectomy), coupled with in vivo MRI-based anatomy of the carotid bifurcation, were used to reconstruct the conditions in vivo, using finite element methods (FEM). The FEM model allows for detailed analysis of mechanical stress/strains and their possible correlation with histologically derived plaque composition in the mechanical stress in the arterial wall.

Specimens were obtained from four patients before undergoing endarterectomy, during which the atherosclerotic plaque was excised, sectioned, and stained for lipid, collagen, smooth muscle cells, and macrophages. By taking a digitized picture of each stained section, the plaque composition was determined and used to construct a two-dimensional replica of the slice using finite element methods. The FEM models incorporated regions of lipid, arterial wall, calcification, and fibrous plaque. Correlations were sought between the histological variables, and physiological variables, (average cyclic strain (CycStrn), average circumferential stress (CircSS), and average effective stress (EffSS)) over each of the slices.

When examining each slice separately, a strong negative correlation was found between macrophage and (CycStrn, CircSS, EffSS). A strong positive correlation was found between smooth muscle cells and (CycStrn, CircSS, EffSS). The results were inconclusive in finding relationships for lipid and collagen.

From this investigation, it can be concluded that macrophage and smooth muscle cell contents are reasonable indicators for detecting areas of high stress.

Thesis Supervisor: Roger D. Kamm
Title: Professor of Mechanical Engineering and Bioengineering

Acknowledgements

I would like to thank Professor Roger Kamm, Dr. Mohammad Kaazempur Mofrad, Ana Isasi, Dr. Galina Sukhova, Hesham Younis, Alyx Chau, Hayden Huang for all the help and guidance they have given me on this project.
From ADINA, I would like to give special thanks to Ted Sussman, Jan, Jian Dong, and Nagi, for their assistance with the Finite Element Modeling.

Table of Contents

1. Introduction

1.1 Background

1.1.1 Heart Disease

Myocardial infarction and Stroke, the principal complications of cardiovascular disease, are the first and third leading causes of death in the U.S. A significant fraction of these catastrophic events are a result of an acute fracture of the diseased arterial wall, leading to subsequent thrombus formation and either the generation of embolic debris or localized occlusion [1]. Almost 61 million Americans (approximately one-fourth of the population) are plagued with heart disease. A majority of the patients suffer from atherosclerosis, or narrowing of the arteries. For these patients, early detection is critical to the prognosis of the disease. Currently there are few non-invasive techniques for assessing the severity of the disease in each patient. Magnetic Resonance Imaging (MRI), ultrasound, and angiography are currently used to determine the degree of stenosis (blockage) of the arteries however there is a need for new technologies that improve diagnostic and prognostic capabilities. While these methods provide remarkably detailed images of the diseased artery, in order to understand the structural consequences of the disease, a different approach is needed. In this these, we propose that the combination of imaging and computational analysis to provide predictions of plaque stability would prove valuable as a diagnostic procedure. This study will focus on determining the link between biomechanical stress in the arteries and the composition of the atherosclerotic plaque.

1.1.2 Atherosclerosis

Atherosclerosis is a form of cardiovascular disease which involves extensive remodeling of the arterial wall, leading to intimal thickening and the formation of lipid pools and regions of calcification.

There have been many different proposed theories as to the cause of atherosclerosis. Some researchers hypothesize that the disease begins with the endothelium, the inner lining of the artery, becoming damaged or dysfunctional [1].

Endothelial cell dysfunction causes low density lipoprotein (LDL) and monocyte entry and modification. LDL is trapped within the subendothelial space and undergoes oxidation. This modified LDL is subsequently ingested by macrophages (differentiated monocytes) which transform into foam cells that, over time, create a region of high lipid content known as the "fatty streak", a precursor of the fibrous plaque associated with more advanced atherosclerosis. This transition from fatty streak to fibrous plaque involves the migration and proliferation of smooth muscle cells. Foam cells stimulate the release of PDGF which causes migration of smooth muscle cells from the media toward the intimal subendothelial space. The foam cells also release cytokines and other growth factors, which cause the proliferation of smooth muscle cells, production of extracellular matrix proteins, and secretion of connective tissue (collagen) by the smooth muscle cells. These mechanisms enlarge the fatty streak and turn it into fibrous plaque.

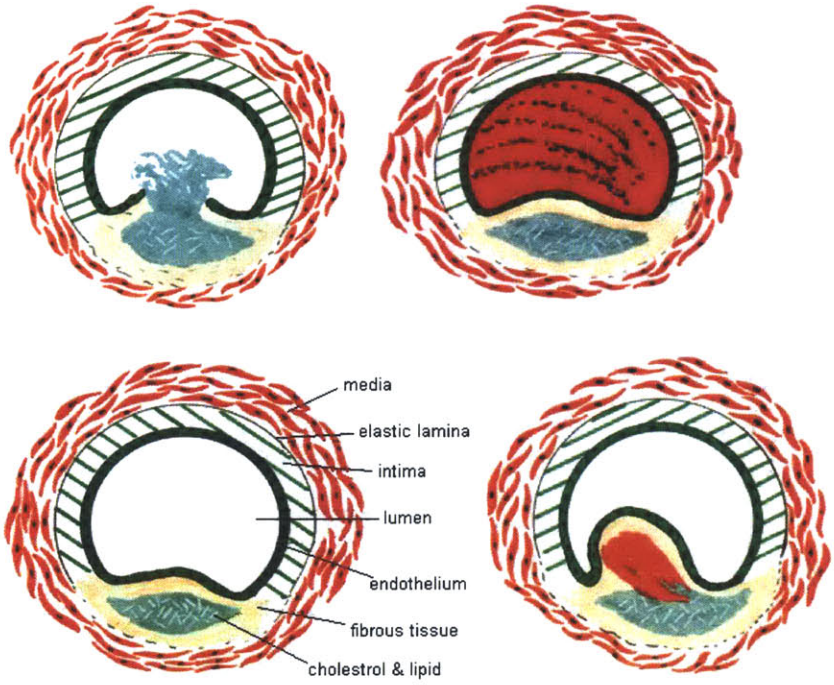

Figure 1: Progression of Atherosclerosis [2]

The arteries become hardened when fatty substances, cholesterol, cellular waste products, calcium, and fibrin are deposited within the arterial wall intima. This leads to a progressive lose of elasticity and as the plaque (atheroma) grows, the lumen of the artery narrows. Disturbance of the fibrous cap, due to the pressure fluctuations within the artery, or possibly due to turbulence near the atheroma can contribute to rupture of plaque as seen in Figure 1. Thrombus formation and, potentially, embolism, can lead to stroke and myocardial infarction, as depicted in Figure 2. In addition to thrombosis and embolic complications, arterial narrowing is itself dangerous to the heart and other vital organs. Arterial blockage has an enormous effect on blood supply to the heart, brain, and extremities. At first as the artery narrows the reduction in diameter has little effect on flow, but as the artery narrows further, the resistance increases dramatically, reducing flow to the distal tissues thereby reducing oxygen supply. The decreased perfusion could cause cells to be deprived of oxygen and accumulate metabolic waste[3].

An anatomical region particularly prone to disease is the carotid bifurcation. Atherosclerosis seems to be prevalent in the bifurcation area due to the complex hemodynamics occurring there. Decreased perfusion or total obstruction of the internal carotid is one of the major causes of stroke. The carotid artery is the major focus of thiis thesis.

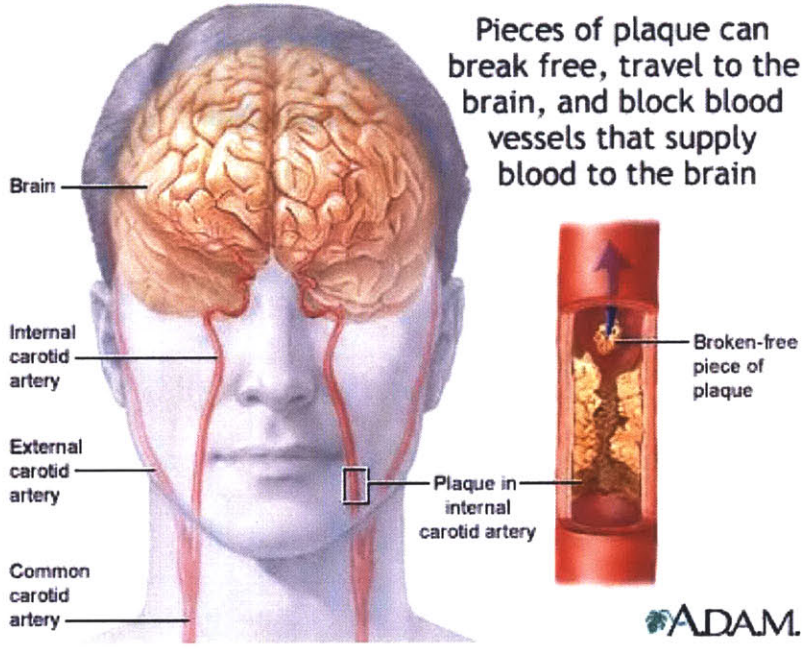

Figure 2: Areas affected by carotid artery flow [4]

1.2 Previous Work

Numerous studies have indicated that mechanical stress/strain leads to the progression of atherosclerosis, however the link between the mechanical factors with the remodeling of the composition of the atherosclerotic plaque remains a subject of considerable debate and a subject of study.

In 1989 Richardson et al. used computer modeling to demonstrate that the distribution of circumferential tensile stress across the intima was greatly altered by the presence of atherosclerotic plaque. Examining the histology they were able to show that

the site of tearing was influenced by variation in the mechanical strength of fibrous cap tissue. The modeling showed that eccentric lipid pools cause stress to be concentrated on the plaque cap and near the edge of the plaque [5], an effect that is accentuated at systole.

Loree et al. used finite element models to demonstrate that the fibrous cap thickness affects the peak circumferential stress experienced by atherosclerotic vessels, further developing the theory that certain morphological configurations were more prone to rupture, leading to the notion of the "vulnerable plaque". This study used cylindrical models as an idealized atherosclerotic coronary artery cross section and then varied the geometry of the plaque in order to determine the effects of fibrous cap thickness [6].

Altered stress levels in the wall of a diseased artery can also have biological impact. Lee et al. studied the distribution of Matrix Metalloproteinase 1 (MMP1) within the arterial wall. MMP1 initiates degradation of collagen, which is one of the major structural components of the extracellular matrix. Finite element methods were also employed to find the distribution of stress in the specimens, while immunohistochemistry was used to determine MMP1 distributions [7]. Their findings led them to speculate that high circumferential stress might stimulate the production of MMP, increasing its concentration locally, thereby weakening the plaque and leading to a predisposition to rupture.

Many studies were conducted to further investigate the role of plaque composition in stress distributions and rupture susceptibility. Cheng et al. found that concentrations of circumferential tensile stress play an important role in rupture, and that variations in plaque material properties might contribute to plaque rupture. This study also

incorporated histology in the construction of a 2-D model of an atherosclerotic cross section of the coronary artery [8].

Huang et al. conducted a study which included the modeling of arterial cross-sections, including plaque composition. However this was performed on post mortem specimens and, as with all models at that time, a constant interluminal pressure of 110mmHg was applied to the model, thereby not accounting for the normal temporal variations in pressure experienced in vivo [9].

Aside from concerns about plaque composition, various other techniques were used to find ways of modeling in-vivo conditions for an atherosclerotic patient. Holzapfel et al. conducted a study incorporating Magnetic Resonance Imaging in order to develop a 3-D Finite Element Model (FEM) to simulate balloon angioplasty. This model incorporated the diseased artery in the FEM model and for the first time in such a model, divided the intima into four sections of fibrous plaque, lipid, calcification, and arterial wall [10].

Zhao et al. found that the coexistence of regions of low wall shear stress and high tensile stress is an important determinant of the formation of atheroma in human arteries. They also incorporated non-invasive magnetic techniques with fluid dynamic and solid dynamics models in order to study regions of wall shear stress and mechanical stress. It was found that the regions which simultaneously experience low wall shear stress and high tensile stress are more prone to atherosclerosis [11].

Delfino et al. extended previous models by incorporating residual strain effects into a three-dimensional FEM of the carotid artery bifurcation. Residual strains were characterized by experimental observation from human and porcine carotid arteries.

However this model was made of homogenous material since their study focused on normal, rather than diseased arteries [12].

1.3 Objectives

As Lee et al. and others have demonstrated, increased biomechanical stresses in the arterial wall can lead to rupture of the fibrous cap [7]. It is also known that stresses within the tissue can themselves lead to arterial wall remodeling, and that stresses can influence the composition of the wall tissue. The objective of this thesis is to investigate the correlation between plaque composition and patterns of mechanical stress, thereby investigating the hypothesis that in-wall stress or strain helps to direct the observed variations in wall composition. If true, this would suggest a new importance for wall stresses, that not only does it induce rupture, but it also alters the distribution of mechanical properties in a way that is either protective (reducing strain magnitudes) or disadvantageous (increasing them). These results might also be used to enhance one's ability to predict stresses and strains and thereby improve our ability to predict the probability of plaque rupture in particular patients.

The need for improved diagnostic and prognostic indicators motivates this study. In order to predict the tendency for plaque rupture, more detailed information in needed regarding the structural properties of the arterial wall and the stresses generated within it during normal variations in blood pressure. In this study, atherosclerotic plaque specimens were obtained from four patients undergoing carotid endarterectomy. The plaque was sliced and stained for Lipid (LIP), Collagen (COL), Macrophage (MP), and Smooth Muscle Cells (SMC). These 2- dimensional specimens, coupled with in vivo MRI-based anatomy of the carotid bifurcation, were used to reconstruct in vivo

conditions, using FEM. The FEM model allows for detailed analysis of mechanical stress/strains and their possible correlation with histologically derived plaque composition in the mechanical stress in the arterial wall. Correlations were sought between physiologic parameters (Cyclic Effective Strain (CyclStr), Circumferential Stress (CircSS), and Effective Stress (EffSS)) and histological parameters (quantification of Lipid (LIP), Collagen (COL), Macropage (MP), and Smooth Muscle Cells (SMC)).

Additionally, this study is among the first to incorporate residual stresses into models of diseased arteries. During carotid endarterectomy, plaque is excised from the artery and removed as one piece. In the process of excision, a longitudinal cut is made along the entire length of the artery, relaxing the internal residual stresses as the artery consequently opens up. Using FEM, the two ends of the artery were brought together using truss elements. This technique was used to incorporate the residual stress experienced in vivo in the artery.

The modeling of the cross sections of the arteries was based on histological data. By taking a digitized picture of each stained slice, the plaque composition was extracted and used to construct a two-dimensional replica of the slice. The models were divided into regions of lipid, arterial wall, fibrous plaque, and calcification.

In Chapter Two, the methods used for analysis of possible correlations between histology and stress/strain are discussed. This chapter explains the procedure for creating FEM's from histology specimens, as well as the method used to quantify the histological parameters in each specimen. Chapter Three presents the results from these studies, and Chapter Four discusses the implications of these results.

2. Methods

This chapter describes the methods used to construct finite element models from histological cross-sections, use FEM to predict the levels of stress and strain within these diseased arterial walls. In addition, histological methods are developed to analyze these same histological sections to identify several of the main biochemical constituents.

In order to study the relation between stress/strain and histological remodeling of the plaque, all parameters needed to be quantified. Average stress/strain values were calculated for each of 16 sectors per slice. This was done using the FEM models created from the digitized pictures of the histology. The stress/strain was compared with a quantified measure of each histological parameter (LIP, COL, MP, SMC) present in each sector per slice. The histological quantification was also taken from the digitized pictures of the excised specimen.

2.1 Excised Plaque Orientation and Staining

In this study the atherosclerotic plaque from four patients was obtained post carotid endarterectomy through an approved human studies protocol. During the procedure, the surgeon made a vertical incision axially along the common and external carotid artery. The internal section of the artery including the thickened intima was removed from the patient intact, and placed in saline solution for a few hours until it could be sliced and stained. The plaque was then cut transversally into sections ranging from 2-15 mm in length. This variability was necessitated by the need to avoid regions with high levels of calcification, which made it difficult to cut in certain areas. Consequently, the samples used in this study will tend to be in regions lacking significant calcification, introducing some degree of bias.

Four thin slices of plaque (few microns in thickness) were cut from each section, and separately stained for COL, LIP, MP, and SMC, which can be seen in Figure 3. One of the four slices was stained for Lipid with Oil Red O solution in 100% propylene glycol, one for Collagen with 0.1% solution of Sirius Red F3BA in saturated aqueous piciric acid, one for Macrophage with CD68 monoclonal antibody anti-surface antigen, and one for Smooth Muscle Cells with HHF-35 monoclonal antibody-α-actin. The four stains were chosen due to the fact that previous studies have shown that few common histological characteristics are universal in atherosclerotic plaque. Lipid, macrophage, collagen, and smooth muscle cell content have been shown to be reliable markers of atherosclerotic progression. Macrophage content is a good indicator due the fibroproliferative process of atherosclerosis which allows an infiltration of monocytes which differentiate into macrophages [1]. As mentioned in the study done by Huang et. al [9], lipid pools are good indicators of mechanical stability of atherosclerotic plaque. Finally, smooth muscle cell and collagen content are also good indicators of atherosclerotic progression, as discussed by Ross [13]

Each of the stained specimens were photographed, digitized and stored as a jpeg file. By combining these four stain pictures, one 2-D model of an arterial cross-section was produced.

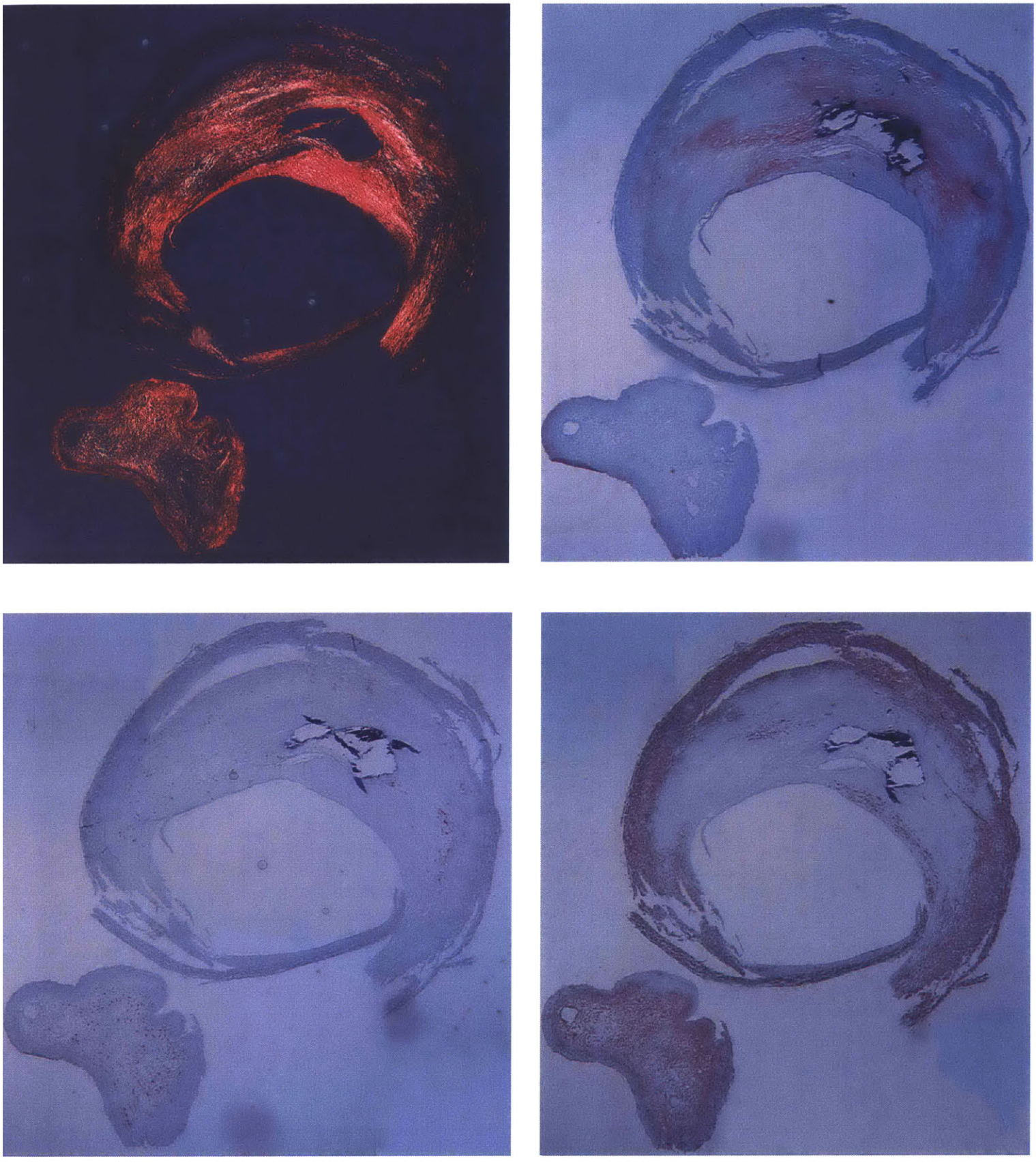

Figure 3: Model 5: Clockwise from top left: Collagen, Lipid, SMCs, and Macrophage

Approximately 5 slices were examined per patient of which, a total of 6 (which are shown in Figure 4) were suitable for reconstruction. Only these six histological sections were modeled due to the ability to reconstruct these specimens as a finite element model without a large deviation from the in vivo structure. The other histological sections were too broken to accurately model the actual specimen. Models which were broken in more than one place were excluded from this study since it would not be possible to construct the relaxed geometry of the specimen. Also, models in which some of the media was missing were excluded since the thickness of the model would significantly decrease in this area. The decrease in thickness would cause there to be large stresses in that area, which would not be an accurate depiction of what is occurring in vivo.

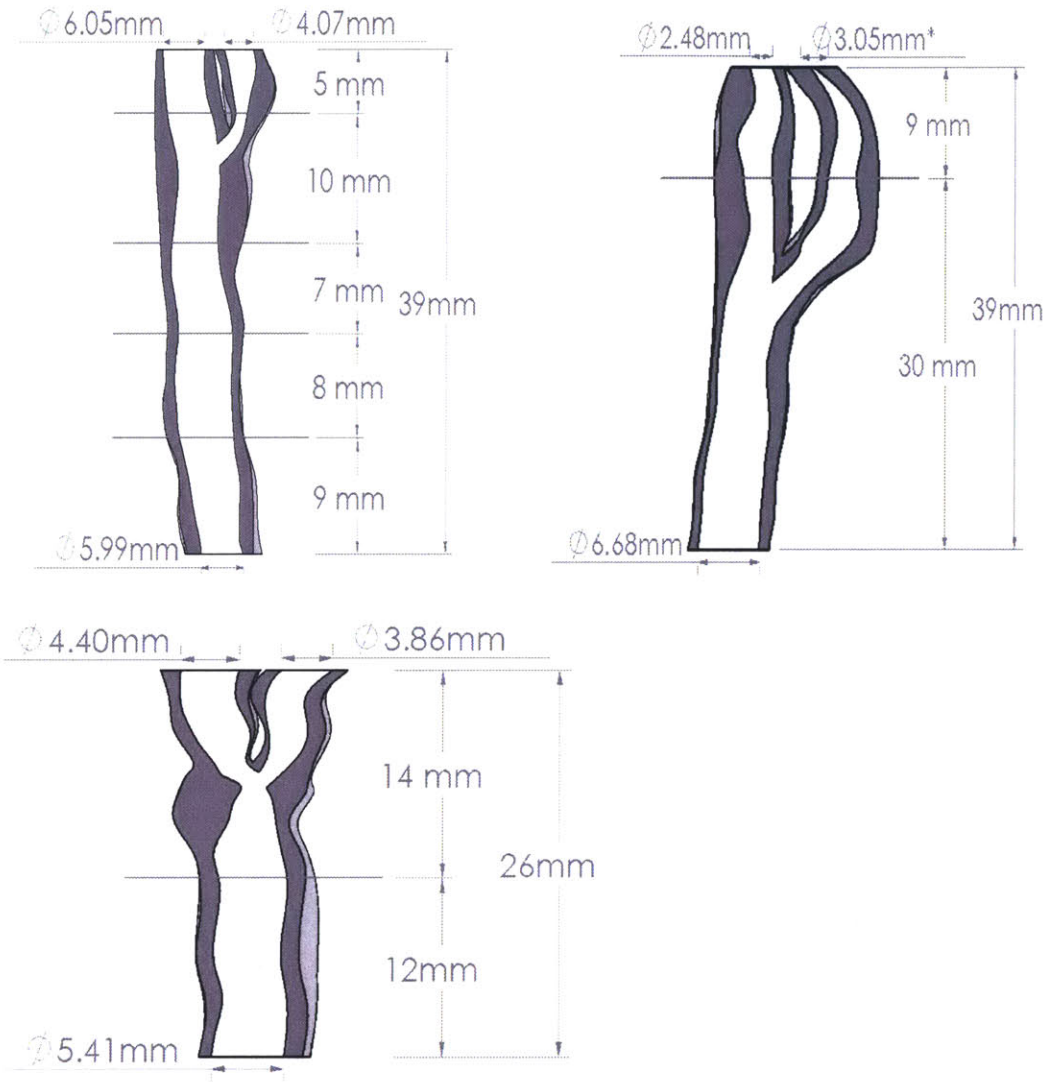

Figure 4: Positioning of the 6 models studied

2.2 Finite Element Modeling

Using the digitized pictures of the stained plaque, the geometry of the specimens was extracted via Optimas v 6.5, a commercial image processing software. Each model arose from the four stainings of the histology. By combining the four stains, one 2-D arterial cross section could be segmented into regions of fibrous plaque, lipid pool, arterial wall, and calcification (Figure 5). These four classifications were chosen since estimates for their material properties were available from previous studies [14,15,16].

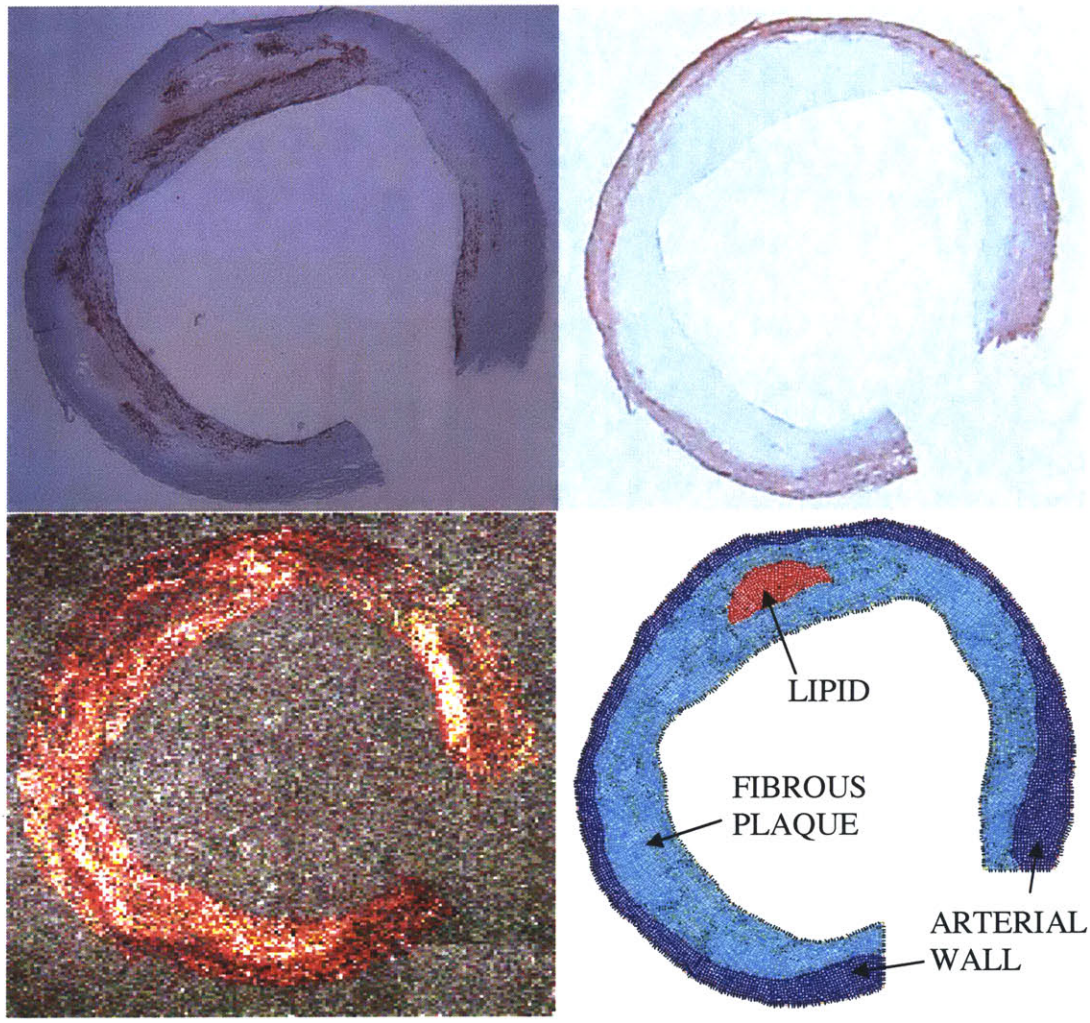

Figure 5: Histology and Mesh of Model 1

Fibrous plaque was assumed to be any region other than lipid, normal arterial wall, or calcification. Specifically, in this model fibrous plaque was identified as that region not clearly identifiable as normal media, lipid pool or calcified. This region typically consisted of macrophages, smooth muscles cells and collagen. Since smooth muscle cells secrete collagen, both stains overlap in many regions. In the histology of this study the macrophage infested areas were also observed to coincide with some regions of smooth muscle cells and collagen, particularly in the region surrounding the lipid pool

and in the region of the fibrous cap. As an example, we show the histology of each section, here stained for macrophage, in Fig. 6.

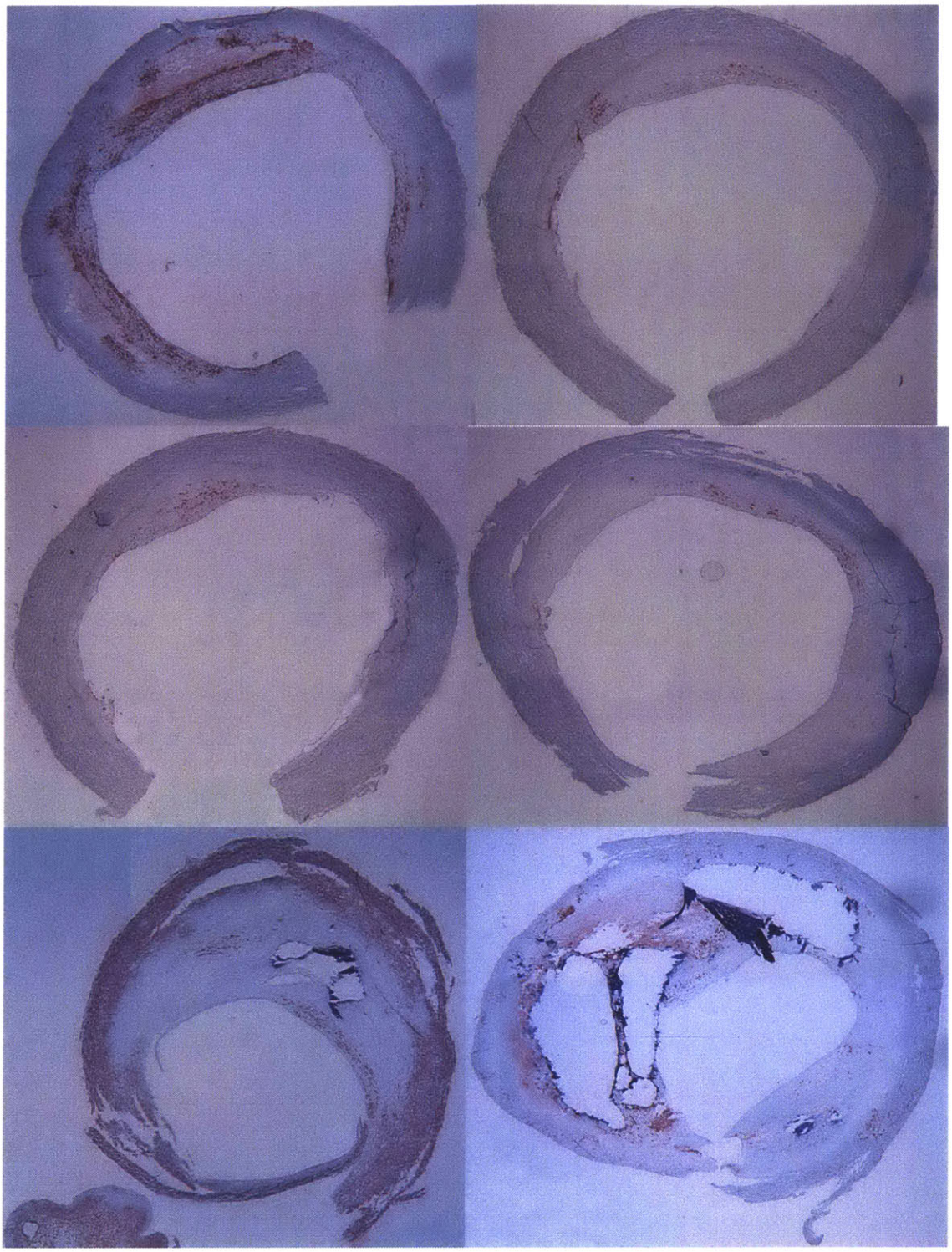

Figure 6 : Macrophage staining for all 6 models. Clockwise from top left: Models 1,2,4,6,5,and 3.

Once the cross section was segmented by drawing boundaries in OPTIMAS, the points which make up the boundaries were imported into the FEM software, ADINA [17], and a mesh was generated.

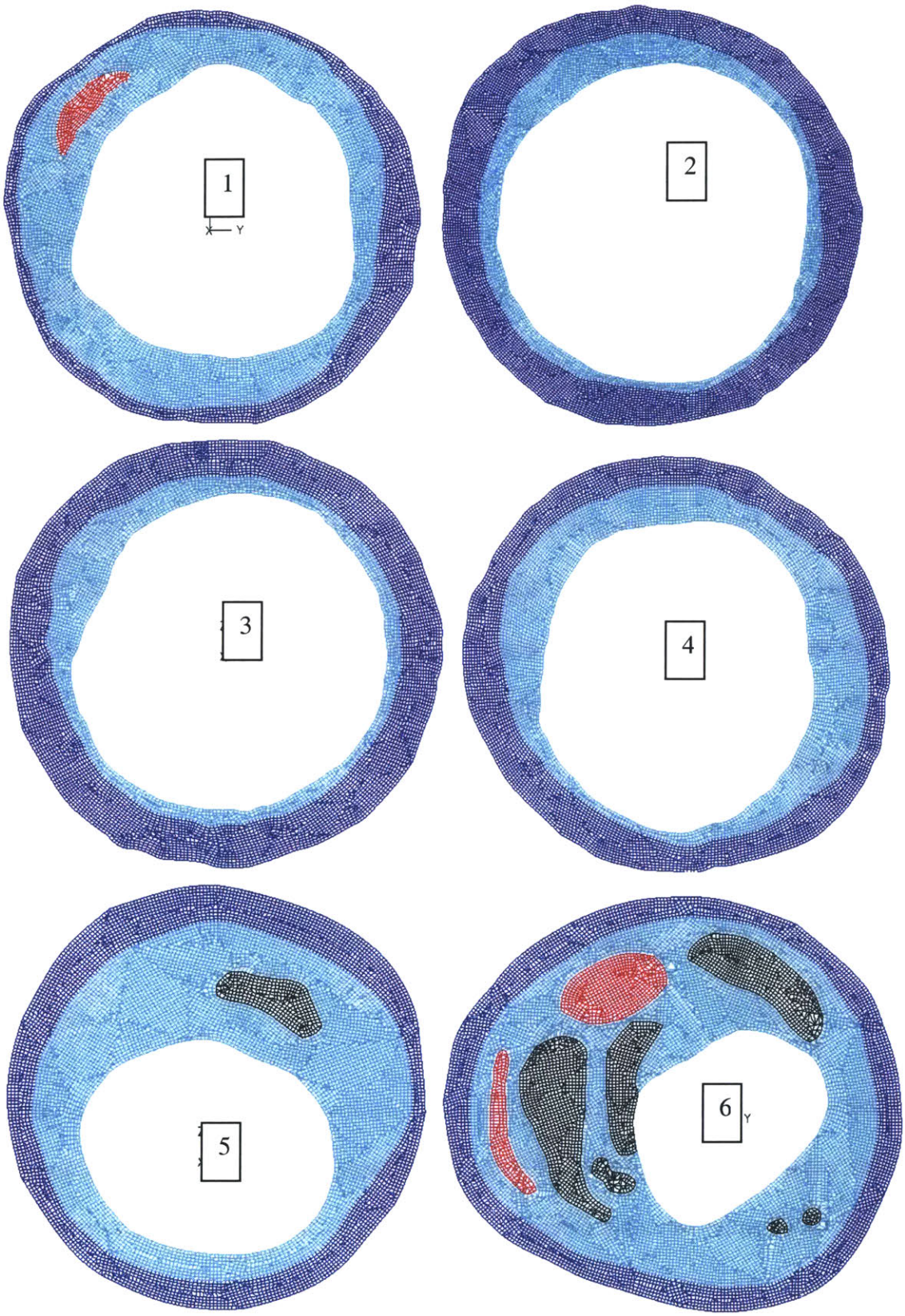

Figure 7: Finite Element Mesh for all 6 models

Nonlinear material properties had to be implemented for this study in order to account for the large stresses and strains. Holzapfel et al [10] characterized biological soft tissue to exhibit a nonlinear stress-strain response with an exponential stiffening effect at higher loads. Anisotropy of the model was not included since ADINA cannot incorporate a nonlinear response with an anisotropic material. Further, not much is known about the anisotropy of lipid pools (which is probably isotropic), fibrous plaque, arterial wall, and calcification.

Another key assumption for the material properties is that of incompressibility. Humphrey [18] claims that an artery can be defined as a "mixture-composite", meaning that it is a solid-fluid mixture. The solid part is composed of smooth muscle cells, collagen and elastin whereas the fluid part is the interstitial fluid that is free to flow within the walls. Under most conditions of interest, particularly those corresponding to normal physiological loads, Humphrey argues it is reasonable to assume incompressibility.

Each of the four regions (lipid, arterial wall, calcification, and fibrous plaque) was assumed to act as a nonlinear, isotropic material and characterized using an isotropic form of the strain energy density function (SEDF)[12]:

$$W = \frac{a}{b}\left(e^{\frac{b}{2}(I_1-3)} - 1\right)$$

where a and b are elastic constants and I_1 is the first invariant strain tensor. In the Taylor series expansion of the SEDF, a has the significance of the elastic modulus and b is related to the strain stiffening behavior of the material. The four materials were modeled as a rubber-like material, defined using Mooney-Rivlin parameters. Mooney-Rivlin materials can be described using two constants, D_1 and D_2, the coefficients for the strain

energy density function. D_1 is proportional to the elastic modulus at zero strain and is equal to a/b, and D_2 characterizes the elastic sensitivity of the material to increasing stress and equals b/2. This parameter incorporates the strain stiffening behavior which was mentioned earlier. These values can be seen below in Table 1.

Tissue Type	D1	D2	Reference
Normal Arterial Wall	2644.7 Pa	8.365	[14]
Lipid	50 Pa	5	[15]
Fibrous Plaque	5105.3 Pa	13	[16]
Calcification	18804.5 Pa	20	[16]

Table 1: Material Properties of regions of atherosclerotic plaque

Each model was a free form mesh, had a mesh density of 0.1 mm, and contained approximately 8000 elements. All of the elements had 9 nodes and were defined to be 2-D solid objects undergoing plane strain. Most were quadrilateral while only relatively few were triangular. The dynamics of the model involved Lagrangian formulation with large displacements and strains [17]. The lines were generated by using Bi-Arcs and Cubic B-Splines. In order to constrain the problem, only Y and Z (in the plane of the model) translation was allowed, and a skew coordinate system had to be applied. To constrain the model, specific boundary conditions had to be applied to the end nodes on each side incision. While one of the end nodes was fixed in the Y and Z direction, the other end node had to be fixed in the direction perpendicular to the incision. This was done by creating a skew coordinate system for that particular coordinate and fixing the appropriate direction.

Each model was run in two stages. The first stage involved the closing of the gap, while the second involved applying the interluminal pressure to the closed model.

2.3 Modeling the Effects of Residual Strain

To account for residual stresses in vivo, FEM commercial software, ADINA (Watertown, MA) [17], was used to bring together the two cut ends of the slice through application of shrinking truss elements (seen in Figure 8) which were modeled as being comprised of a non-linear thermo-elastic material. Thermal properties were assigned to the truss elements and appropriate temperatures were applied to bring the truss elements to a zero length. This involved the assignment of a Young's Modulus of 10^{10} Pa so that once the truss elements shrunk to a length of zero, it was practically ensured that the gap would not open up again when the interluminal pressure was applied.

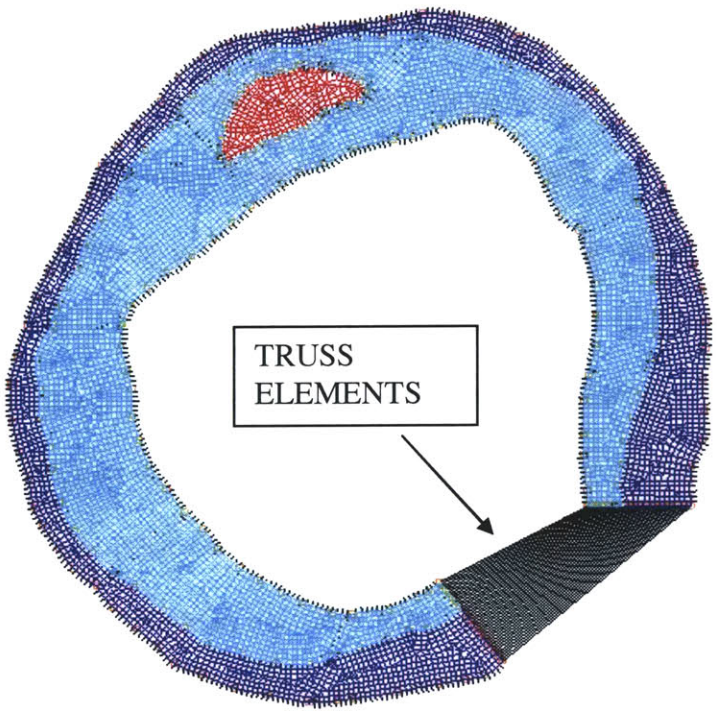

Figure 8: Truss Elements in Model 1 used to close the gap

After closing the gap, introducing normal residual stresses, a pressure loading was applied as a boundary condition on the interior boundary of the arterial slice. The interluminal pressure was ramped from 0 mmHg to the patient specific systolic pressure over approximately 30 steps, depending on the complexity of the model.

Models were also run without residual stress. This was done using the same two part scheme, however after closing the gap, the residual stress/strain which was generated, was then erased. After the deletion of the stress, the interluminal pressure was applied to a closed, yet relaxed model.

Figure 9 demonstrates the effects of residual strain. Residual stress/strain is such that the inside of the annulus is in compression and the outside of the annulus is in tension. If residual strain is not incorporated in a model, this means that the annulus was in a relaxed state initially. This causes a much higher stress gradient throughout the thickness of the annulus, and neglects the fact that the inner part of the annulus was initially in compression when residual stresses are present.

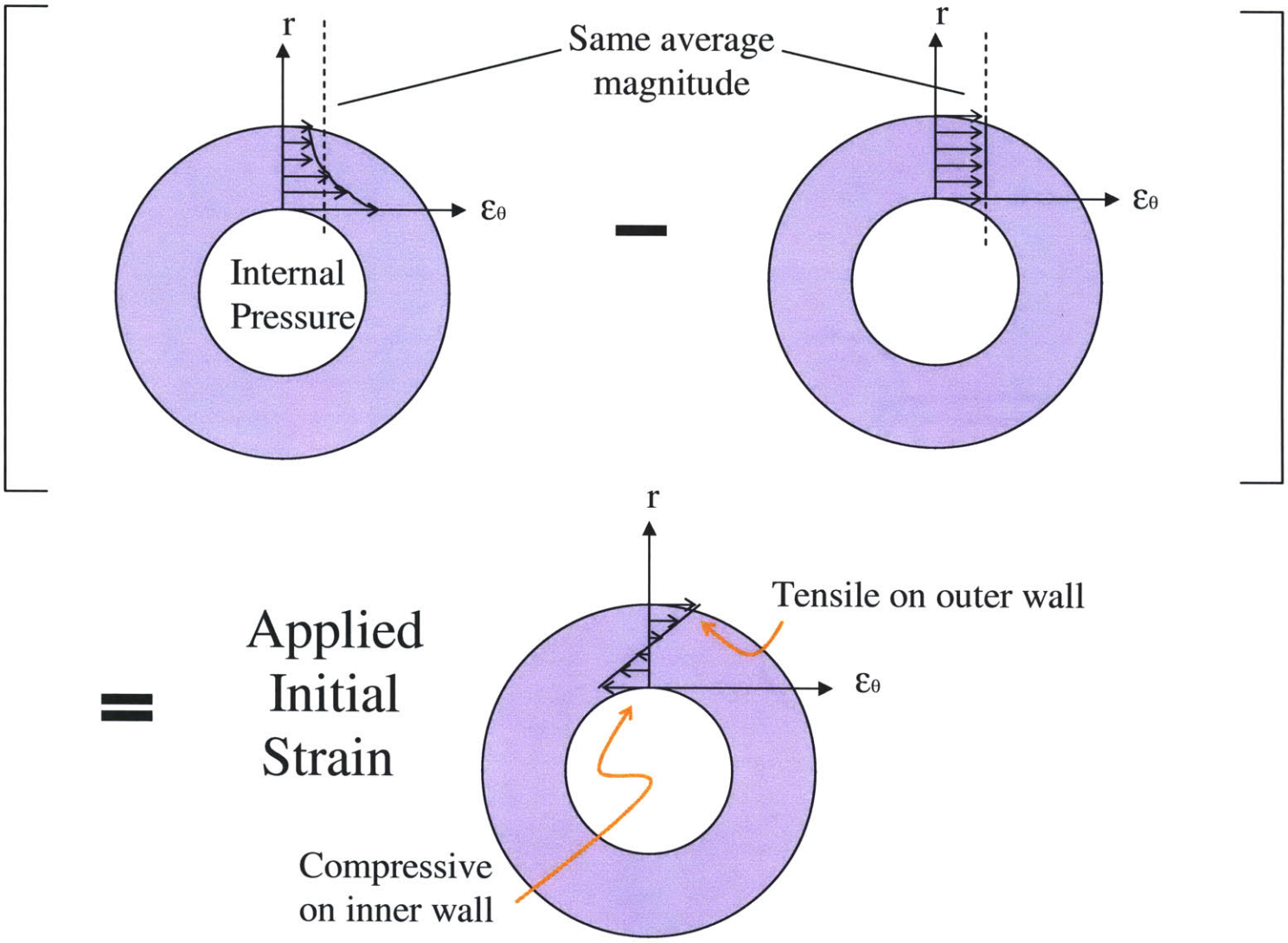

Figure 9 : Effect of Residual Strain

2.4 Correlations

The central objective of this study was to search for possible correlations between the histology and the stress/strain patterns in the same specimen. For this purpose it was necessary to quantify the composition of the specimen as well as the stress/strain. Consequently, the specimen was divided into 16 segments of 22.5 degrees and the comparisons between stress/strain and composition were based on the resulting circumferential distributions. While the choice of 16 segments was arbitrary, it seemed a reasonable compromise providing some degree of circumferential discretization yet not exceeding the resolution of the quantitative data.

In order to assure accuracy and consistency, the right end of the surgical incision of the plaque marked 0 degrees and the left most end of the cut specimen was labeled as 360 degrees.

2.4.1 Histology Quantification

OPTIMAS was used again into to quantify the amount of each histology parameter. In a jpeg image, the color composition scheme is RGB (red, green, blue), and all staining reagents used in this study stain red for for the particular constituent. Quantification is accomplished in the following way: the user specifies a pixel on the image that is considered to be red to a high degree of certainty, and a threshold is selected that will mark in yellow any pixel whose red component is higher than that of the specified pixel . The pixels in the image that have been marked yellow are taken to correspond to SMCs. Figure 10 below shows sample images of excised specimen sections that have been stained with their corresponding collagen, macrophage, lipids and SMC pixels, respectively, marked in yellow, as obtained following the method described above [19].

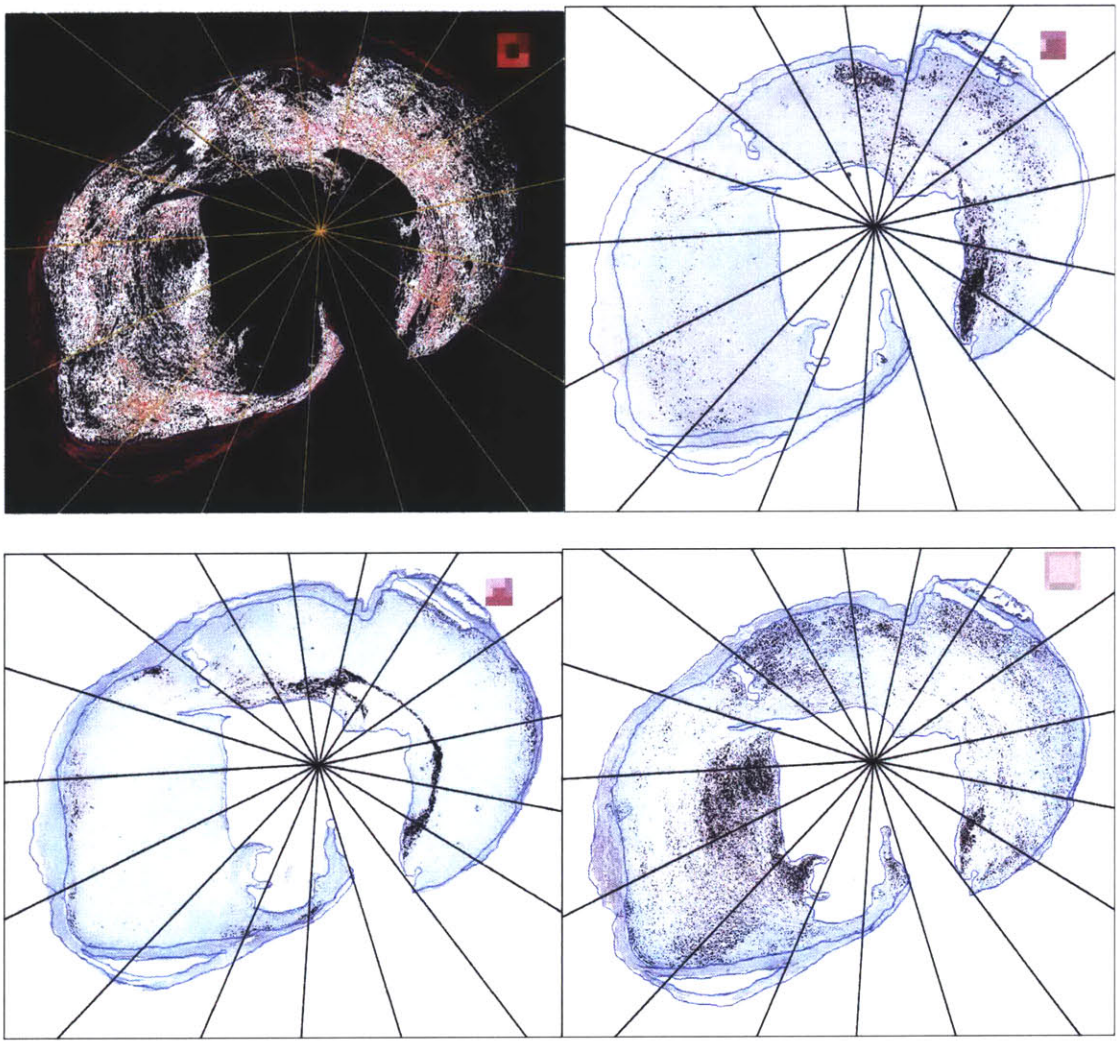

Figure 10: Quantification of relevant components of histology. Clockwise from top left: Collagen, Macrophage, Smooth Muscle Cells, and Lipid

The histology variables (LIP, COL, SMC, and MΦ) were examined over the intimal layer of the slice and were recorded as an absolute value of the number of pixels which contained the stain, and as a percentage (stained pixels/ total pixels of the 22.5 degree intimal sector of the slice).

2.4.2 Physiological Parameter Quantification

The same analysis was done for physiological variables (average cyclic strain (CycS), average circumferential stress (CircSS), and average effective stress (EffSS)) over each of the 16 sectors. Using the coordinates of the origin (center of the lumen) from the

OPTIMAS histological quantification scheme, we were able to maintain a large degree of accuracy between the FEM model and the histology. After obtaining the coordinates of the origin, the circumferential angle, θ for the finite element model was determined by extracting the position of the nodes. Hence, the FEM sectors matched up exactly with the histological sectors. After ordering the nodes by θposition (0 →360), a few physiological variables (σ_{xx} ,σ_{yy} ,σ_{xy} ,ε_{xx} ,ε_{yy} ,ε_{xy}) were extracted and following characteristic values (stress and strain invariants) CycS, CircSS, and EffSS were computed.

$$CyclicStrain = \frac{\varepsilon_{xx}+\varepsilon_{yy}}{2} + \sqrt{\left(\frac{\varepsilon_{xx}-\varepsilon_{yy}}{2}\right)^2 + \left(\frac{\gamma_{xy}}{2}\right)^2}\,(systole) -$$

$$\frac{\varepsilon_{xx}+\varepsilon_{yy}}{2} + \sqrt{\left(\frac{\varepsilon_{xx}-\varepsilon_{yy}}{2}\right)^2 + \left(\frac{\gamma_{xy}}{2}\right)^2}\,(diastole)$$

$$CircumferentialStress = \frac{\sigma_{xx}+\sigma_{yy}}{2} + \frac{(\sigma_{xx}-\sigma_{yy})}{2}(\cos(2\theta)) + \tau_{xy}(\sin(2\theta))$$

$$EffectiveStress = \frac{\sigma_{xx}+\sigma_{yy}}{2} + \sqrt{\left(\frac{\sigma_{xx}-\sigma_{yy}}{2}\right)^2 + (\tau_{xy})^2}$$

The nodes were then grouped into 16 sectors based on their θ position : (0→22.5, 22.5→45, 45→77.5, etc.). Each of the three physiological variables was then averaged over the node in each sector. Finally, correlations were sought between the absolute quantification of the histological variables, and the physiological variables.

2.4.3 Regression Analysis

Since the variables in question (LIP, COL, SMC, MΦ, CycS, CircSS, and EffSS) are not normally distributed, non-parameteric statistical methods, which make fewer assumptions about the shape of the distribution, must be used. In this investigation the data happen to be ordinal. Ordinal data can be ordered but do not have specific numerical values which arithmetic can be performed on to provide an insight into the data. For this type of data a Rank-Order Correlation is the most appropriate method of finding a correlation. The Spearman rank-order correlation is different from trying to fit the data to a line, because the rank-order uses relative measurements of the data as opposed to the usual linear measurements. This correlation test is basically an ordinal measure of association between two variables. The test tries to find a monotonic relationship between two variables. A monotonic relationship occurs when an increase in one variable is accompanied by an increase (or decrease) in the other variable. For example, If *X2* > *X1,* then *Y2* >= *Y1* for a monotonic increase. If *X2* >*X1* then *Y2* <= *Y1* for a monotonic decrease. The strength of this monotonic relation can be expressed by the correlation coefficient, **r**.

The Spearman rank order correlation coefficient and its corresponding significance test [20] were employed to find the correlations between each pair of variables (one histological parameter and one physiologic parameter). The Spearman rank order correlation is the analog for ordinal data to the Pearson correlation coefficient:

$$r = 1 - \frac{6\sum(D^2)}{n(n^2-1)}$$

where D is the difference in the rank of pairs x and y, and n is the number of pairs. Basically, the x and y variables are rank ordered separately. Then the differences between the ranks of both variables are calculated (D= Rank (x)-Rank(y)).

The corresponding significance test was used to determine if the correlation coefficient was generated randomly. All correlations with a p-value of ≤ 0.05 were considered to be significant. The level of significance is calculated by checking all the permutations of ranks in the data set and counting the fraction for which the r values of the permutations are more extreme than the r values found for the non- permutated data set. Since this is not very practical as the number of permutations grows proportional to $N!$, for $N > 10$ usually only a random subset of the permutations is actually checked.

3. Results

3.1 Stress/ Strain Distribution

From approximately 30 specimens, 6 were modeled and studied due to the inability to reconstruct the rest. Model 1 had only a lipid core, model 5 contained only calcification, and model 6 contained lipid cores and calcification. Lipid pools were important to examine due to the fact that they were by far the softest of the 4 materials which were used to model each specimen. Likewise areas of calcification were also interesting since those areas were the stiffest of the 4 materials. It was also interesting to look at the location of the lipid pools and areas of calcification, since their proximity to the lumen played a significant role in the stress/strain distribution throughout the specimen. While model 1 had a large fibrous cap separating the lumen from the lipid pool, model 6 had a relatively small cap, which separated the calcification from the lumen.

The maximum values of CycStrn, EffSS, and CircSS were examined for each model. In some cases, the maximum values were caused by mesh deformities which results in stress/ strain concentrations. In those cases, the average value of stress/ strain in that area was examined. The average value was calculated as the average stress/ strain over the two elements which caused the stress concentration. These values can be seen in Table 2.

	CycStrn		CircSS (Pa)		EffSS (Pa)	
Model	Max	(max avg)	Max	(max avg)	Max	(max avg)
1	0.1869	**0.1124**	532984	**360750**	492755	**325267**
2	0.07891	**0.062**	601412	**393318**	581486	**366020**
3	0.08712	----------	875607	**474941**	852802	**427499**
4	0.07876	----------	485437	**285425**	460510	**254651**
5	0.07785	**0.05533**	261083	--------	248463	---------
6	0.1064	**0.0586**	580113	**190904**	612906	**198751**

Table 2: Maximum Values and Average Maximum Values of Cyclic Strain, Circumferential Stress and Effective Stress

3.1.1 Cyclic Strain

Cyclic Strain, expressed as the strain invariant defined in Methods, was an important physiological variable to examine, since biological remodeling tends to be triggered by temporal variations, as opposed to a constant increase or decrease, in stress/strain. Variations in effective strain were examined between diastole and systole, and it was found that maximum strain occurred at systole and minimum strain occurred at diastole. Consequently, using the effective cyclic strain will accurately indicate regions of increased strain amplitude. We expected the cyclic strain to be largest in the areas of lipid pools and smallest in the areas of calcification due to the material properties mentioned previously. We also expected the cyclic strain to be greatest in the inner area of the plaque due to the large stresses this area undergoes. The inner area of the plaque experiences more stress than the outer region due to geometrical reasons which will be explained in further detail in Discussion.

The models that contained lipid pools (models 1 and 6) experienced highly localized maxima in cyclic strain of approximately 5-11 %. These large values were in a very localized region of the lipid pools and could be attributed to the material properties of lipid which characterize it as a very soft material.

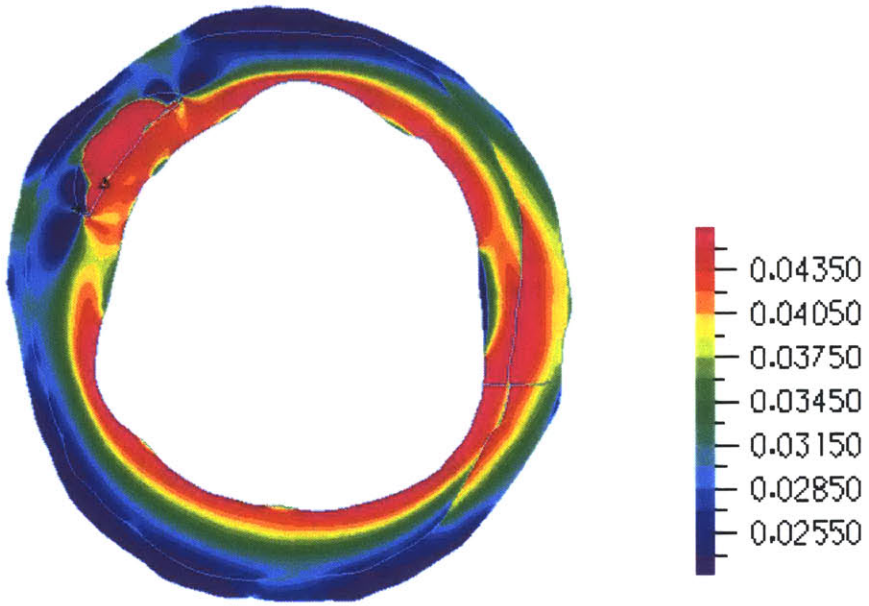

Figure 11: Cyclic Strain for Model 1; Δ denotes max, * denotes min

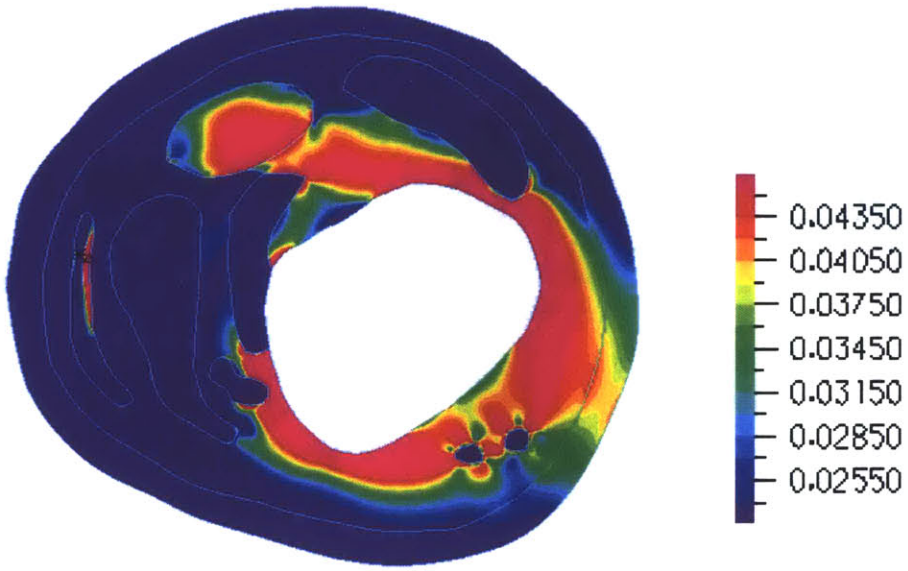

Figure 12: Cyclic Strain for Model 6; Δ denotes max, * denotes min

It is interesting to note that both these models also had a region in which the cyclic strain was out of phase with the pressure, which indicated that effective strain in/ near the lipid area was greater during diastole than during systole. As mentioned before, a time variation analysis of the effective strain was performed and it was found that effective strain generally increases between diastole and systole. Since this negative cyclic strain was found in a very localized region of the model, it was thought to be possibly due to an artifact of the mesh that did not affect the rest of the solution.

Areas of calcification were present in Models 5 and 6, which caused there to be less strain in the regions outside of those calcified nodules.

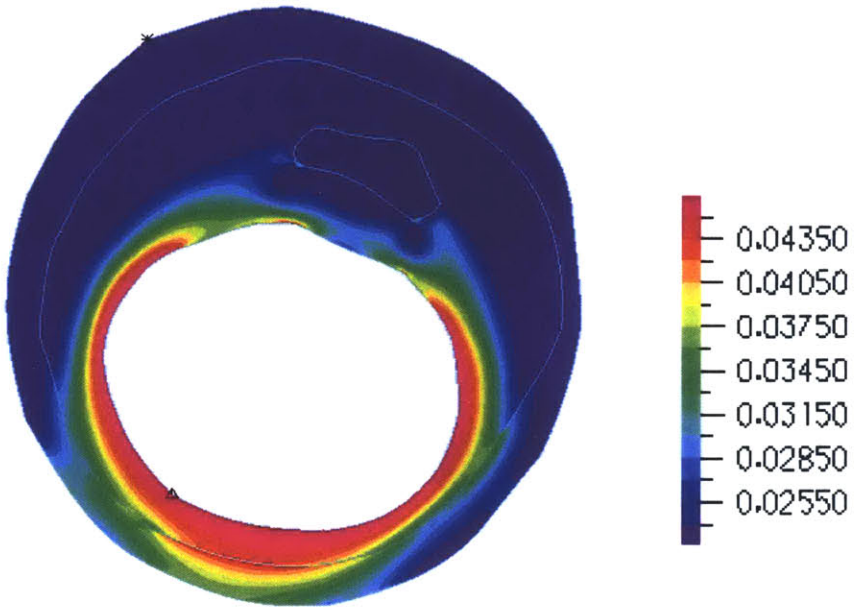

Figure 13: Cyclic Strain for Model 5; Δ denotes max, * denotes min

Model 5 had a maximum cyclic strain of 5% which coincided with the maximum cyclic strain found in Model 6. This suggests that the effect of calcification on strain is stronger than the effect of lipid on strain. Although Model 6 had two lipid pools, they did not seem to experience the same high cyclic strain that the lipid pool in Model 1 experienced. This can be attributed to the presence of calcification in Model 6.

Unlike the lipid models, the specimens without lipid or calcification (Models 2,3, and 4) seemed to exhibit the greatest cyclic strain directly opposite to the atheroma at a location where the wall was relatively thin. The maximum cyclic strain seen in these three models was approximately 6-8% and lay on the border of the lumen. These values occurred in localized regions of the specimens, yet were still significant in determining the vulnerable areas of the plaque. It was often the shoulder region of the plaque which sustained the high strains. Although the fibrous plaque was modeled as stiffer than the arterial wall which surrounds it, the fibrous region still exhibited the greatest strain since this area tends to be located near the inner boundary of the artery and consequently

experiences the most stress. As mentioned previously, the inner circumference undergoes higher strain than the outer circumference due to geometrical reasons, which will be explained in Discussion.

3.1.2 Effective and Circumferential Stress

The circumferential stress in the artery is an important indicator of the potential for plaque rupture [7]. The effective stress was computed as well as the circumferential stress however the differences between the two were generally small. Since the circumferential stress is the primary component in the effective stress then it is reasonable to see why the data are similar for both stresses. The circumferential stress values were slightly lower than the effective stress values, however the trends seen in the specimens were identical.

The location of the maximum stress was on the lumenal border for all of the models. Over all the models the entire fibrous plaque region felt an average effective stress of approximately 50 kPa, whereas the surrounding arterial wall region experienced 10-20 kPa. This is due to a larger circumferential stress being experienced in the inner wall of the artery for geometrical reasons. As mentioned earlier, the inner wall expands more than the outer wall and will consequently have higher levels of circumferential stress and effective stress.

In order to assess the validity of these solutions one can make an estimate of the stress felt in this arterial "pressure vessel". Using $\sigma = PR/t$, where σ = the circumferential stress in the pressure vessel, P= the interlumenal pressure (120mmHg ~ 16000 Pa), R= radius of the vessel (.005m), and t= thickness of the wall (.001m), the calculation gives σ = 80,000 Pa, as a conservative estimate. This result can be seen to coincide with the

results seen in Figure 14. Most of the fibrous plaque region undergoes stress in excess of 100,000 Pa.

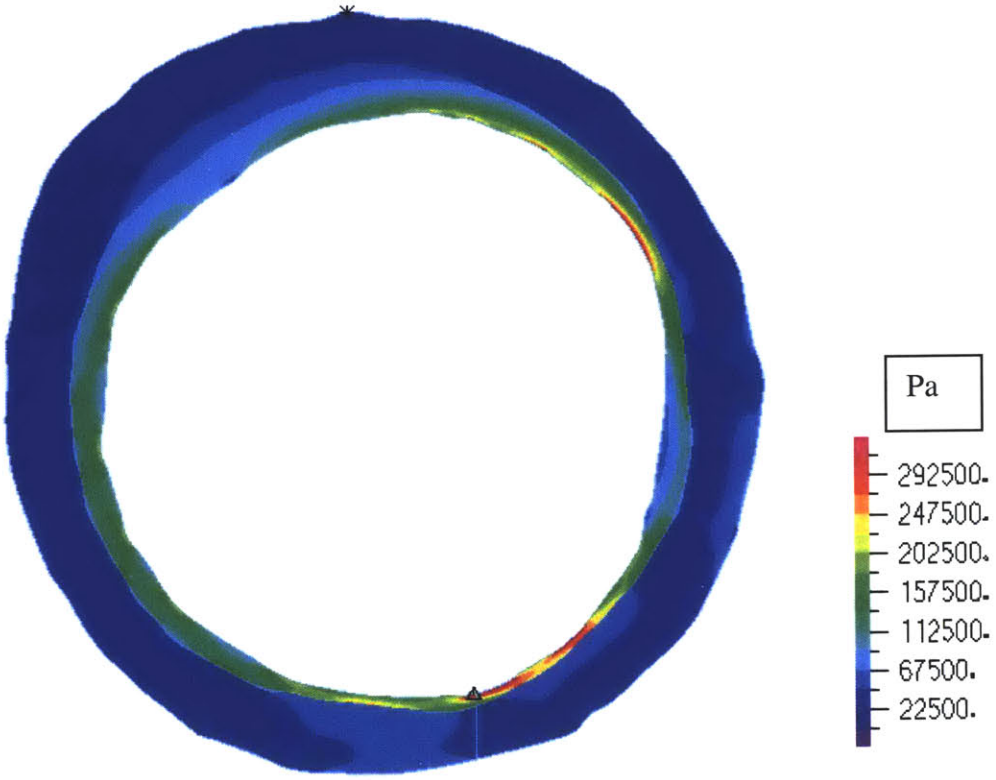

Figure 14: Effective Stress of Model 2 at Systole; Δ denotes max, * denotes min

Model 1 had a lipid pool, which was a region of extremely low effective stress due the soft and compliant nature of lipid pools.

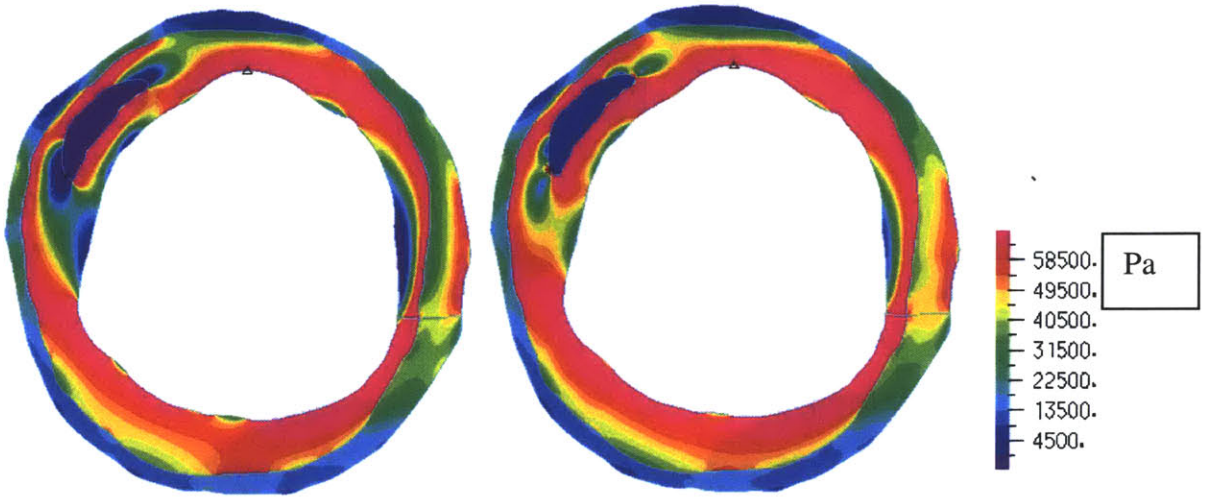

Figure 15: Circumferential (left) and Effective Stress (right) for Model 1; Δ denotes max, * denotes min

The region surrounding the lipid pool however, took on much higher stress since the "effective" thickness of the artery had been reduced. This is evident from Laplace's Law which states that as the thickness of a vessel decreases, the stress increases to compensate [21].

Models without lipid or calcification (models 2-4) experienced averaged maximum effective and circumferential stresses between 250 kPa-475 kPa. Similar to the maximum cyclic strain values presented earlier, these maximum stresses were in localized regions on the border of the lumen.

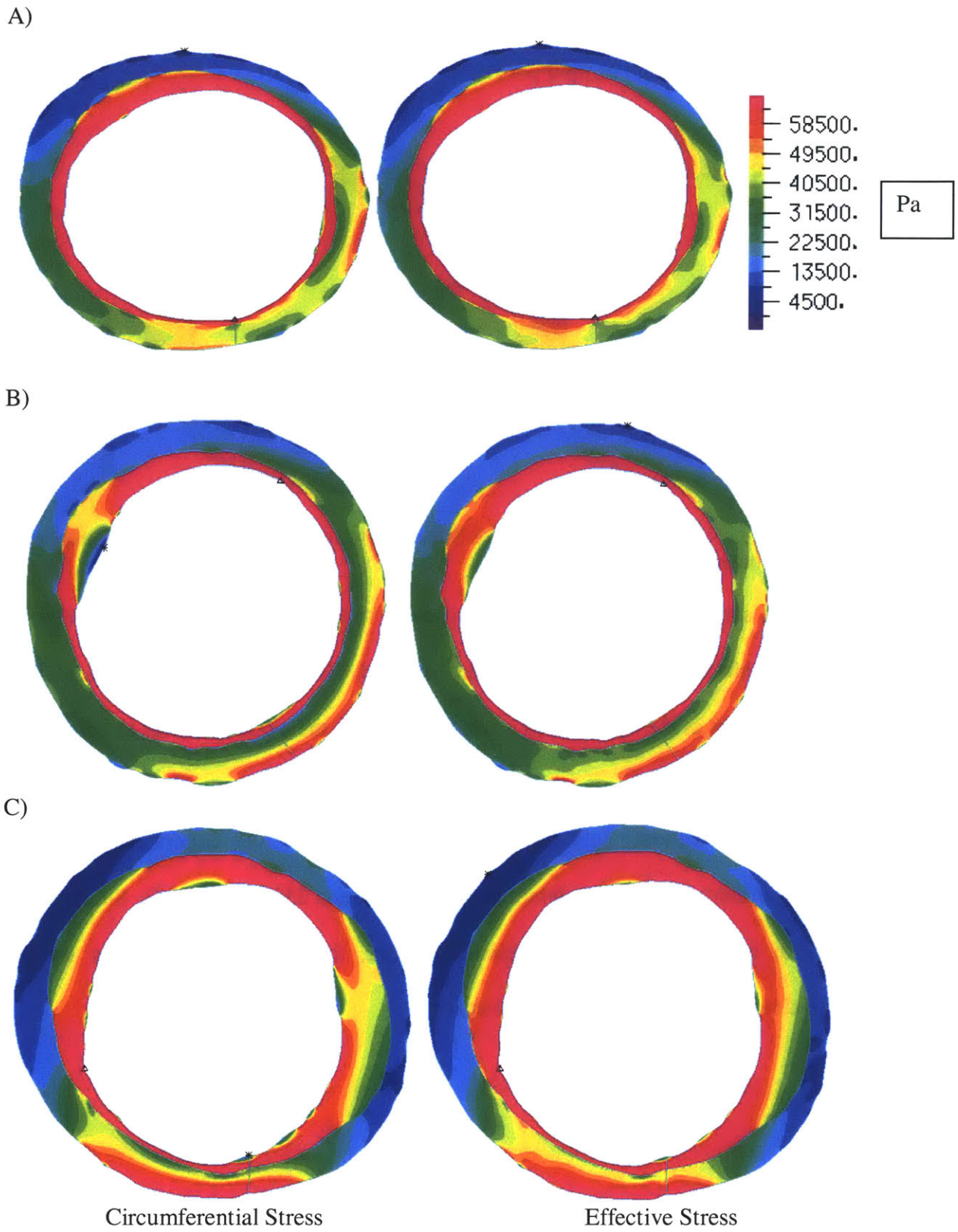

Figure 16: Circumferential (left) and Effective Stress (right) for Models 2,3, and 4 (A,B, and C, respectively); Δ denotes max, * denotes min

Models that contained calcification (models 5&6) experienced a maximum stress of approximately 200 kPa. Both models had relatively thick walls and large areas of calcification, which led to small strains and stresses throughout the mesh. The maximum stress in Model 5 was distributed largely over several sections of the lumenal border, whereas the maximum stress in Model 6 was in a very localized region.

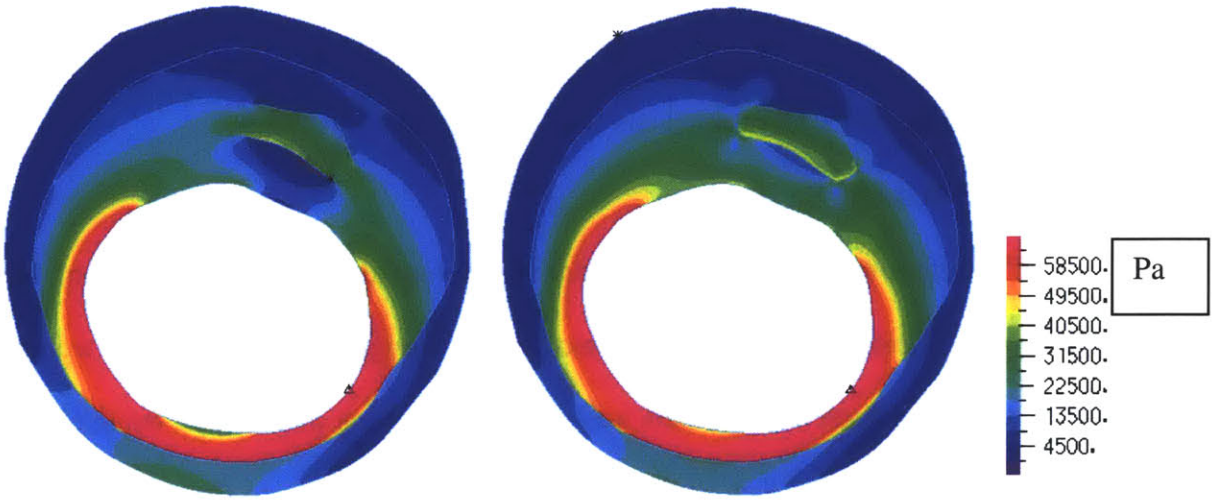

Figure 17: Circumferential (left) and Effective Stress (right) for Model 5; Δ denotes max, * denotes min

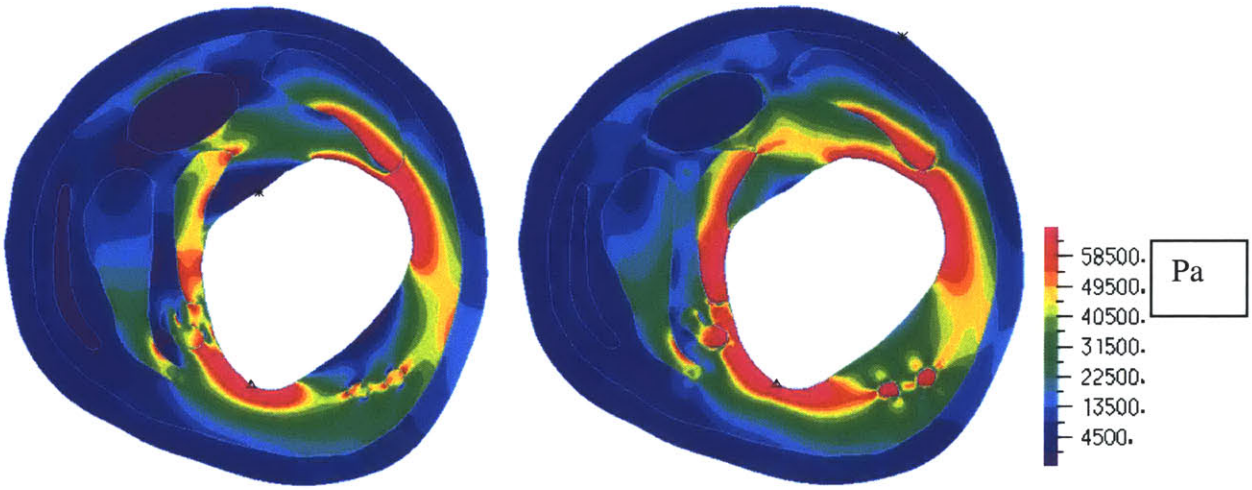

Figure 18: Circumferential (left) and Effective Stress (right) for Model 6; Δ denotes max, * denotes min

Model 6 had both lipid and calcification, yet still had areas of low stress in the lipid regions. The calcification tended to decrease the strain experienced in the region outer to the calcification and hence these low strain regions also experienced low stress. The areas of calcification also supported the greatest stress since they were close to the lumen and constituted the stiffest material in the plaque.

The effect of residual strain was also investigated in this study. Often times the residual strain/ stress is neglected when modeling histology. A few models were simulated with and without residual strain to examine its significance.

3.2 Effect of Residual Strain

The effect of incorporating residual strain was also investigated in 3 of the 6 models. All six models were not used since it was thought that three models would be sufficient to study these effects. This was done by removing the residual strain obtained from closing the gap, and then applying an interluminal pressure to the closed specimen in the same manner as was done for the same specimens with residual strain. One model contained a lipid pool, whereas the other two consisted only of fibrous plaque and arterial wall. These models were compared to the original model which contained residual strains.

A)

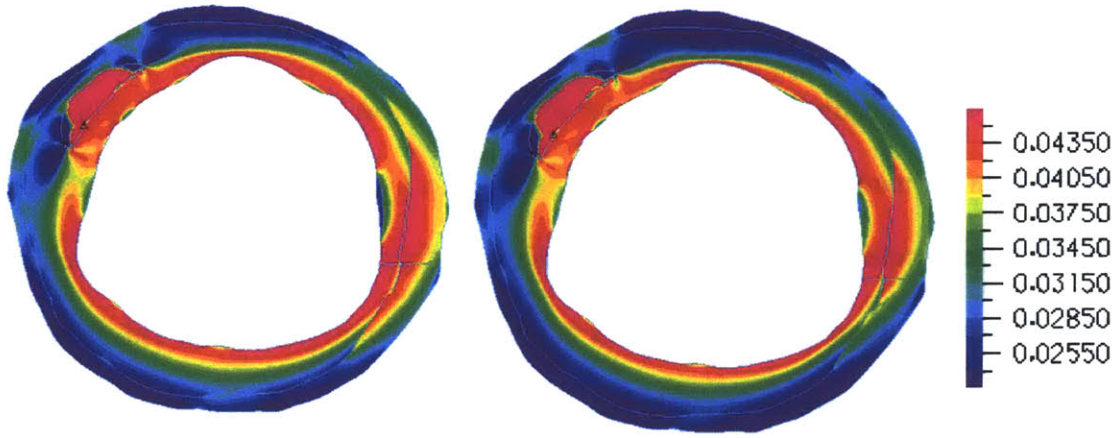

Cyclic strain with Res. Strain Cyclic Strain without Res. Strain

B)

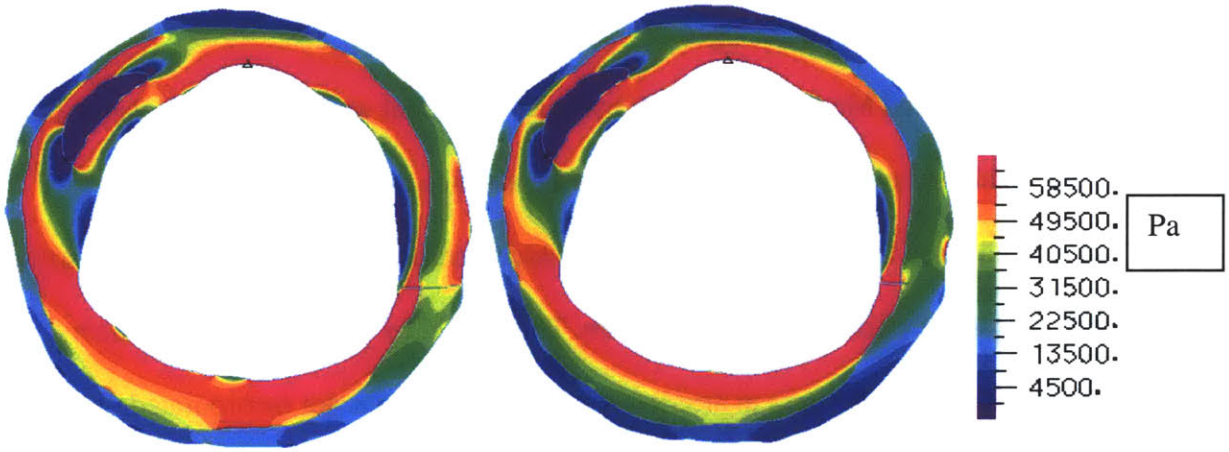

Circumferential Stress with Res Strain Circumferential Stress without Res Strain

C)

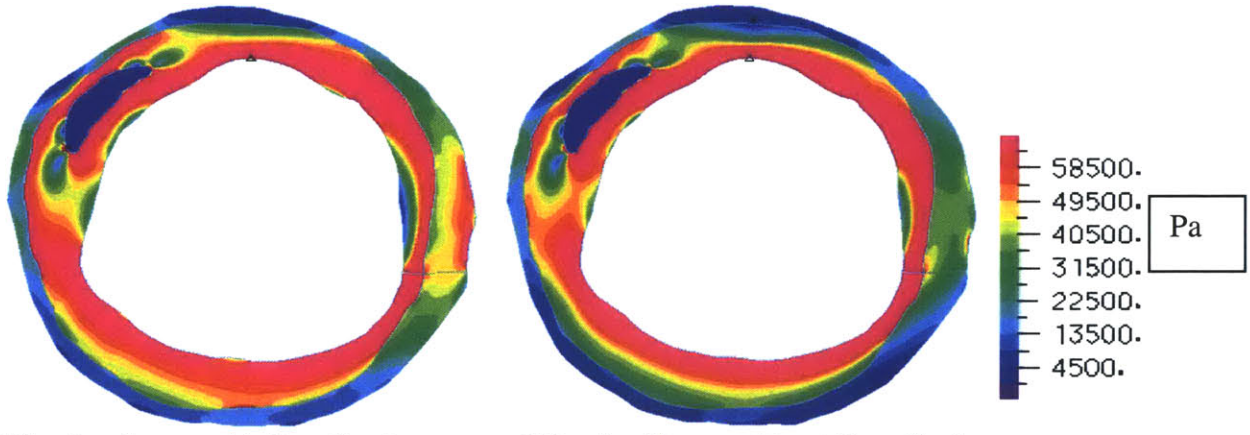

Effective Stress with Res. Strain Effective Stress without Res. Strain

Figure 19: Cyclic Strain, Circumferential Stress, and Effective Stress (A,B, and C, respectively for Model 1; Left= With Residual Strain, Right= Without Residual Strain; Δ denotes max, * denotes min

Note from this comparison that the presence of residual stress/strain lessens the stress/strain gradient across the vessel wall and makes the stress profile more uniform. This is due to the profile of residual stress/ strain which was explained in detail in Methods. In the model without residual strain, the effective and circumferential stress had a much larger gradient of stress across the thickness of the wall. The maximum cyclic strain appeared to have approximately the same distribution in both cases. This is most likely due to the fact that cyclic strain is an amplitude and not an absolute measure. Since the effective strain gradient would be steeper during diastole as well as systole, the difference would remain unchanged.

Model 2 and Model 3 were both made up of arterial wall and fibrous plaque only, and also exhibited a larger stress gradient in the absence of residual strain.

In all three models, the presence of residual strain helps to homogenize the stress profile across the thickness of the specimen. This would be crucial in studies which examine the maximum stress in arteries. If residual strain was not incorporated, the maximum stress would be higher than that which was experienced in vivo.

Model2

A)

Cyclic strain with Res. Strain Cyclic Strain without Res. Strain

B)

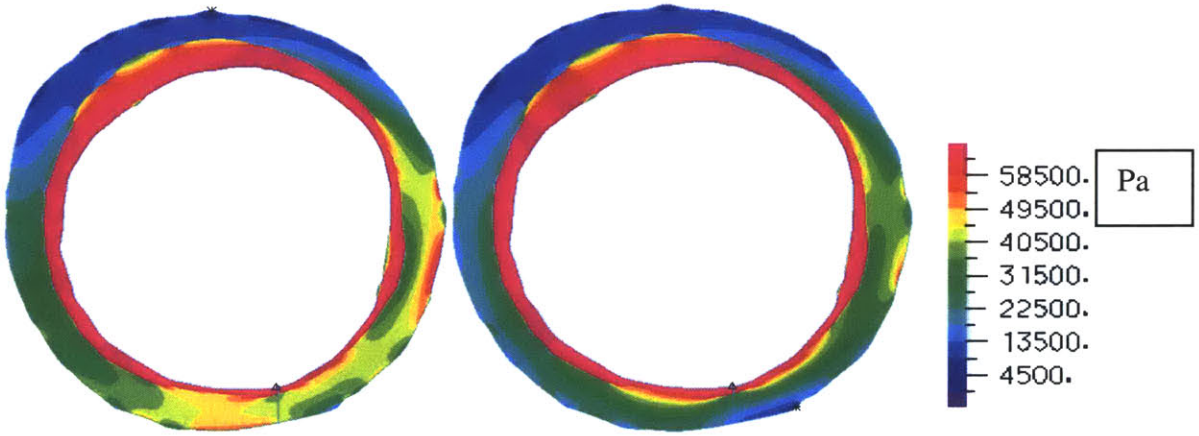

Circumferential Stress with Res Strain Circumferential Stress without Res Strain\

C)

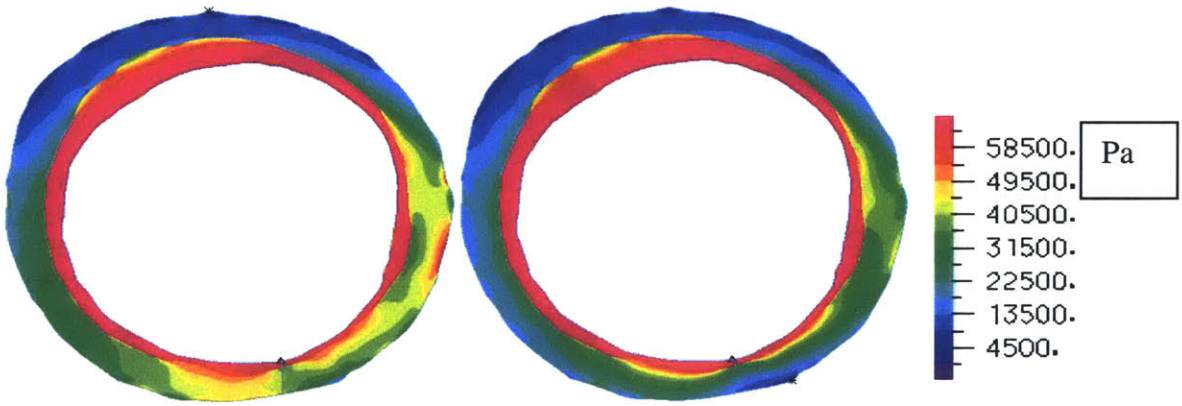

Effective Stress with Res. Strain Effective Stress without Res. Strain

Figure 20: Cyclic Strain, Circumferential Stress, and Effective Stress (A,B, and C, respectively for Model 2; Left= With Residual Strain, Right= Without Residual Strain; Δ denotes max, * denotes min

Model 3

A)

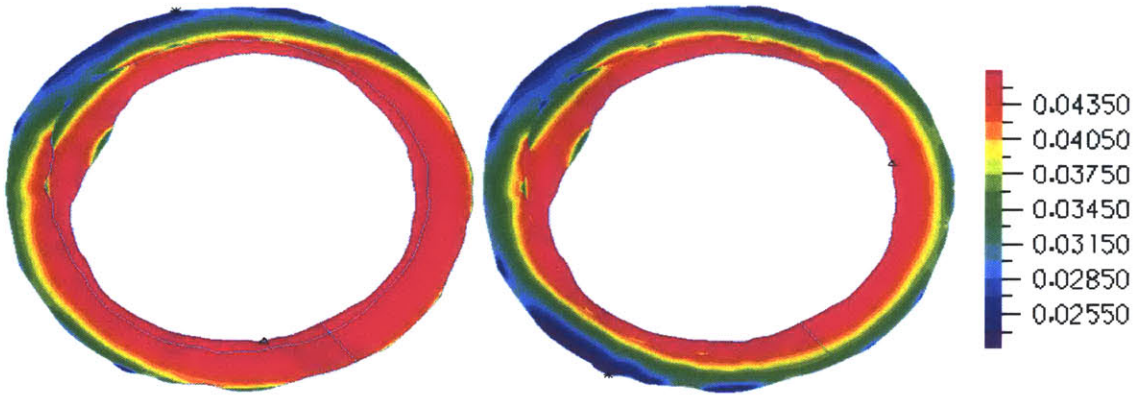

Cyclic strain with Res. Strain Cyclic Strain without Res. Strain

B)

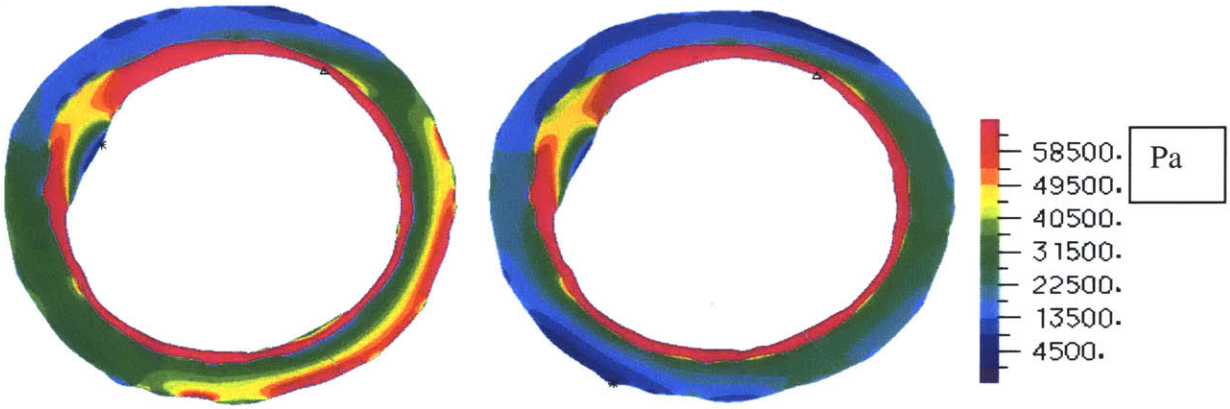

Circumferential Stress with Res. Strain Circumferential Stress without Res. Strain

C)

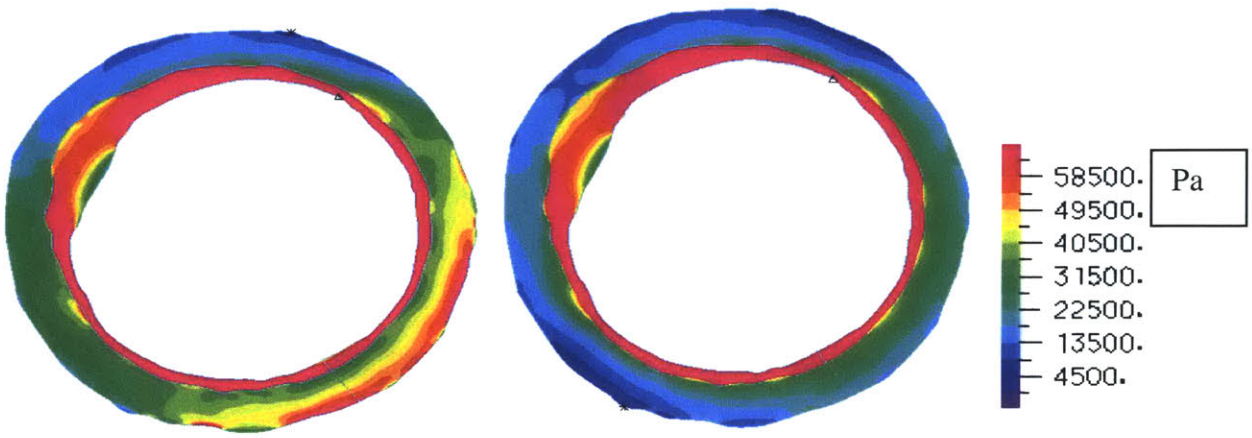

Effective Stress with Res. Strain Effective Stress without Res. Strain

Figure 21: Cyclic Strain, Circumferential Stress, and Effective Stress (A,B, and C, respectively for Model 1; Left= With Residual Strain, Right= Without Residual Strain; Δ denotes max, * denotes min

3.3 Circumferential Variation

After building Finite Element Models of each specimen, the circumferential variation of the histological and physiological components was examined for trends. The data for the histology was obtained by using an image processing software, OPTIMAS, and quantifying the amount of each relevant component (Smooth Muscle Cells, Lipid, Macrophage, and Collagen). This is was discussed at length in Methods, and the raw data can be found in Appendix A. The physiological components (Cyclic Strain, Circumferential Stress, Effective Stress) were obtained from the Finite Element Model and averaged over each 22.5 degree sector. The raw data for the physiological parameters can also be found in Appendix A. Since it had been decided that the normalized quantification of histology was of more significance than the absolute quantification , only the normalized histology was plotted and analyzed in this section.

Model 1 contained a lipid pool, and exhibited a positive trend between lipid and strain.

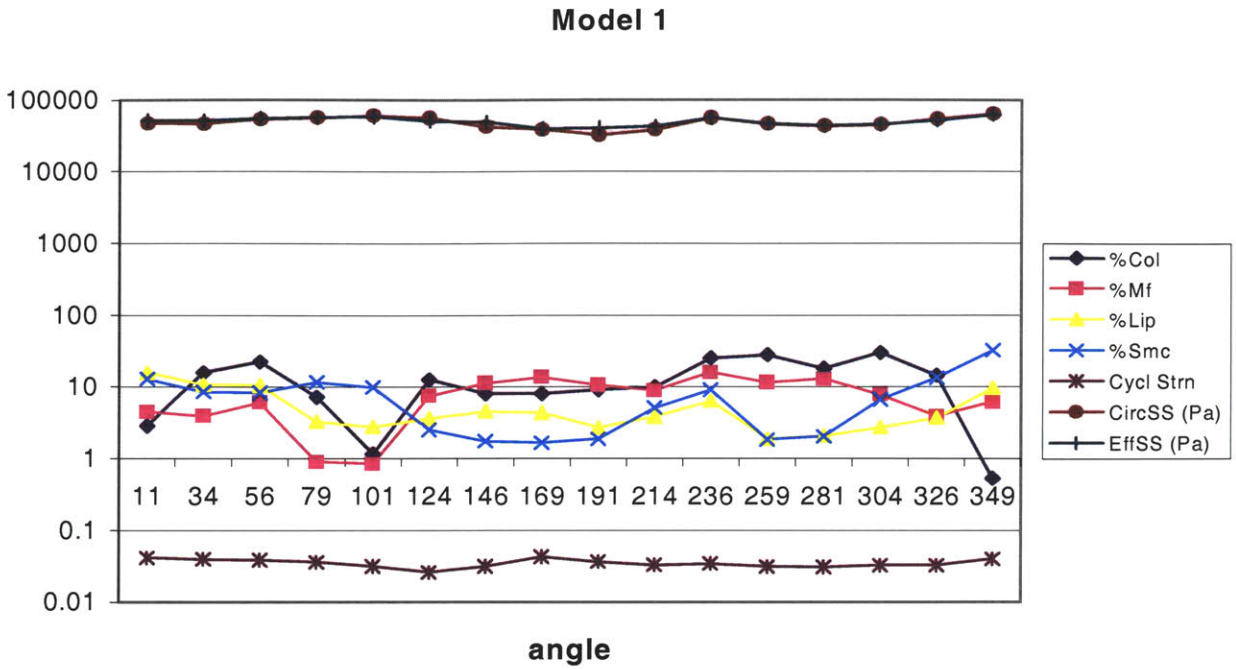

Figure 22: Circumferential Variation of % histology components and physiological variable for Model 1

This simply demonstrates, however, that large strains are associated with lipid pools due to their low stiffness. This trend was not expected to be seen since the quantification of lipid involved intracellular and extracellular lipid (lipid pools). In this study the amount of intracellular lipid should not have had much of an effect on the stress/ strain whereas the extracellular lipid should have had an effect due to its drastically different material properties. Due to this inconsistency a meaningful trend was not expected to be found. However, since this model in particular contained a large amount of extracellular lipid, the correlation accurately described the extracellular lipid vs strain relationship.

Models 2 and 3 were located below the bifurcation and were composed of fibrous plaque and arterial wall.

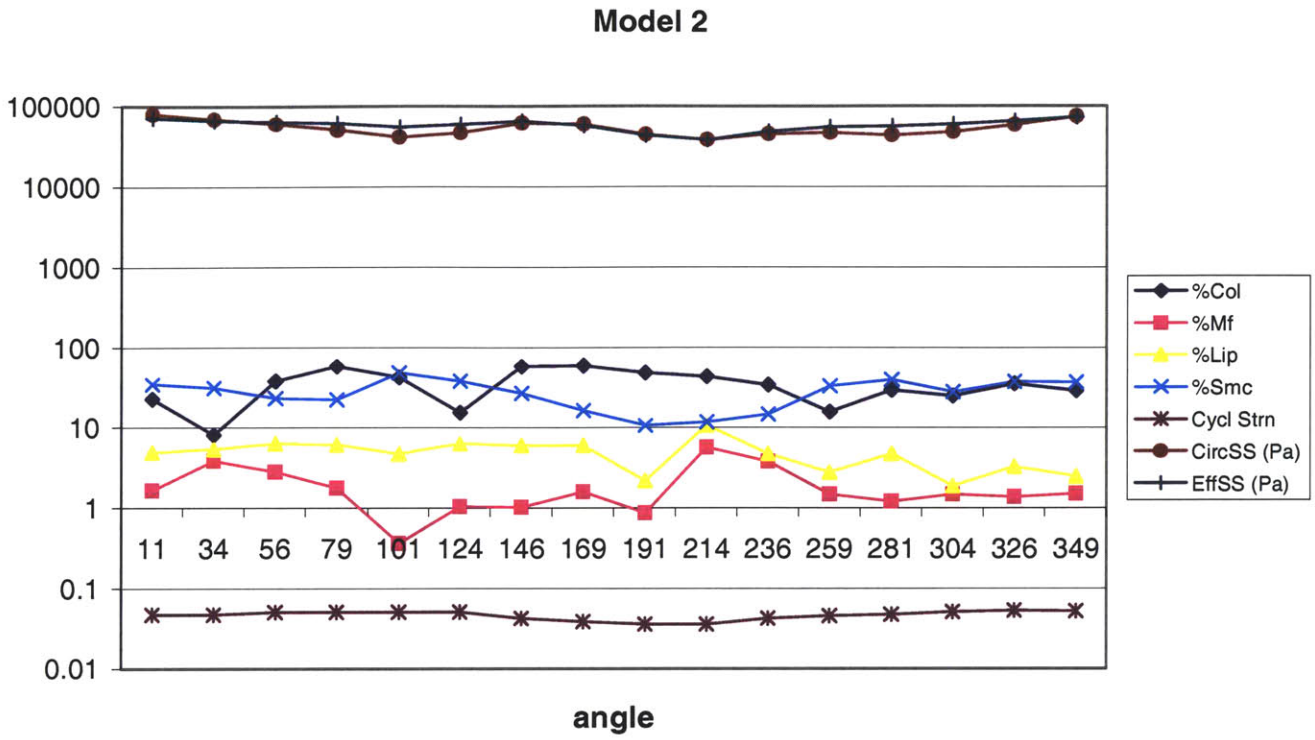

Figure 23: Circumferential Variation of % histology components and physiological variable for Model 2

Model 2 showed significant positive relationships only between SMC and CyclStrn. Since Model 2 was not very diseased there was not much LIP and MP present, and instead was comprised mainly of SMC and COL.

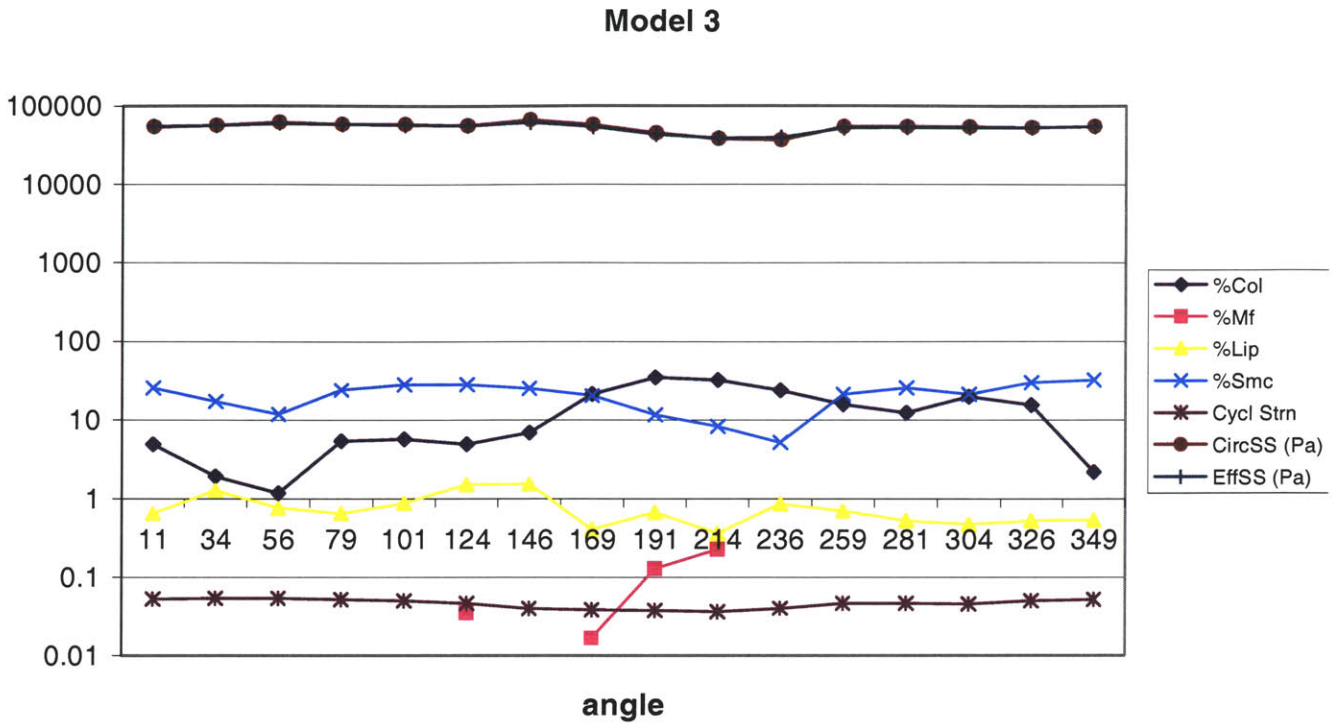

Figure 24: Circumferential Variation of % histology components and physiological variable for Model 3

Model 3 exhibited a strong negative correlation between MP concentration and CycStrn. However this model also did not have much macrophage content. This can be seen since there were only four macrophage quantities which can be graphed. The rest of the sectors contained 0% macrophage. Hence, any relationship found with macrophage was not too meaningful for this model.

This model also showed a positive correlation between LIP and CircSS/ EffSS. Unlike Model 1, this model contained only intracellular lipid and no extracellular lipid. It is important to note that when a majority of the lipid is found in lipid pools (extracellular), this forces there to be a positive correlation since the Finite Element Modeling characterizes the lipid pools to be regions of low modulus. Therefore, only correlations found in vessels without lipid pools can be viewed as meaningful.

Consequently, the lipid relationship in this model was meaningful concerning the role of lipid in the remodeling process. Model 3 also showed a negative relationship between collagen and CycStrn / EffSS / CircSS.

Models 4 and 5 were located closer to the carotid bifurcation of the patient, and are located below and above the bifurcation, respectively. Model 4 contained only fibrous plaque and normal arterial wall. Of the four histology components, collagen had the most similar distribution to the physiological parameters, and it varied out of phase with the CyclStrn and EffSS. Hence Model 4 showed a negative correlation between COL and CyclStrn/ EffSS.

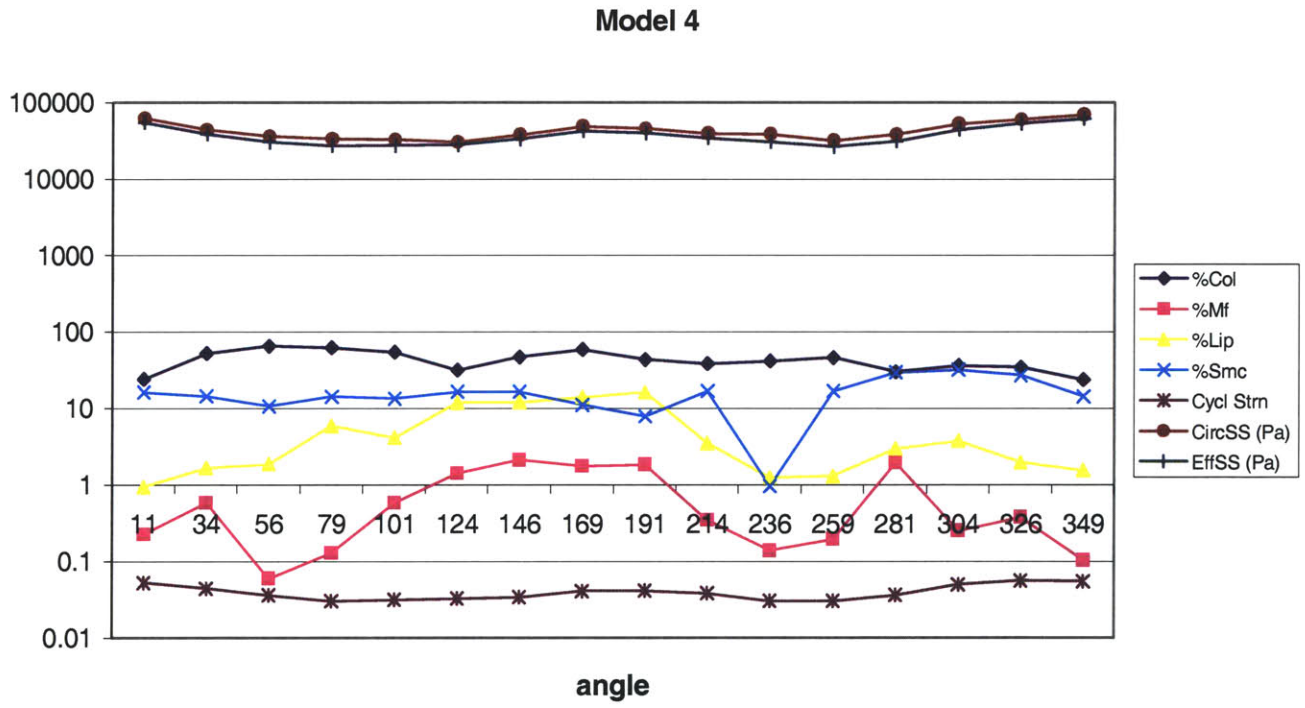

Figure 25: Circumferential Variation of % histology components and physiological variable for Model 4

Model 5 contained a calcification nodule, as well as fibrous plaque and arterial wall.

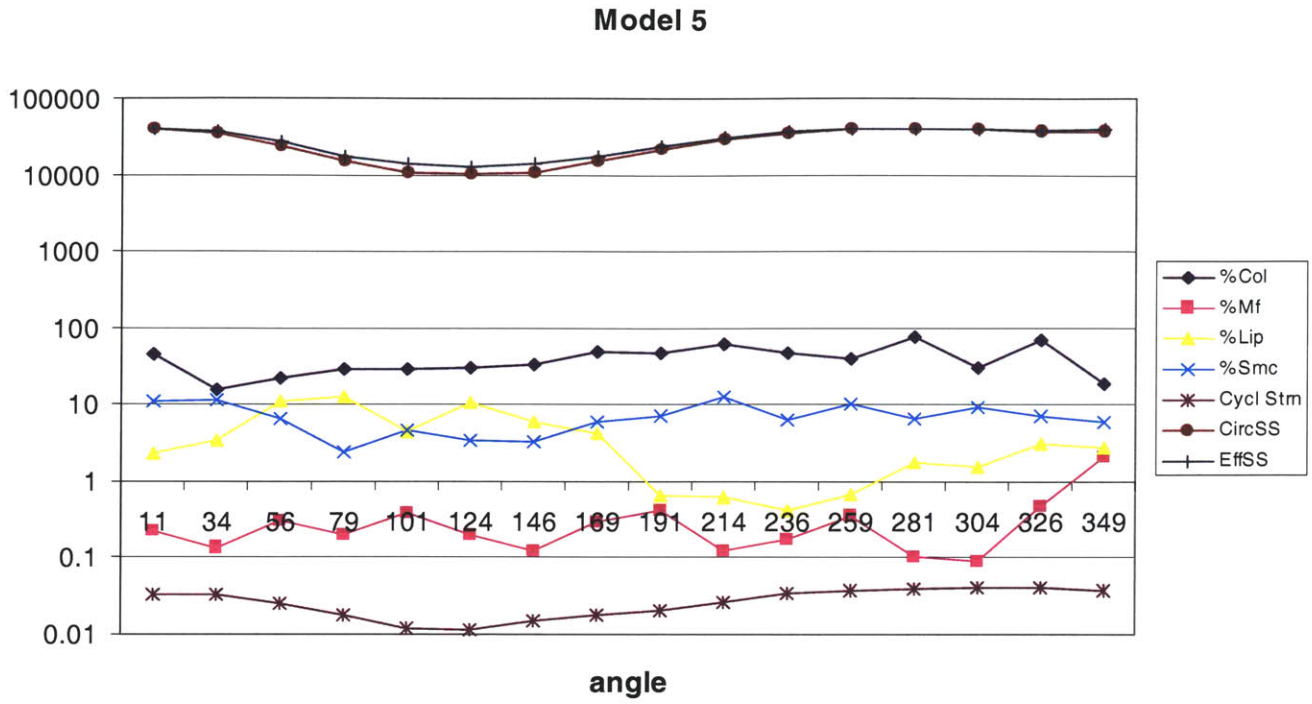

Figure 26: Circumferential Variation of % histology components and physiological variable for Model 5

Model 5 exhibited a positive correlation between Smooth Muscle Cells and CyclStrn / CircSS / EffSS, and a negative correlation between Lipid and CyclStrn/ CircSS/ EffSS. Previously a positive correlation was seen in Model 1, which contained extracellular lipid. As explained previously, since this model did not have any lipid pools to force a positive correlation between LIP and CyclStrn / CircSS / EffSS, the lipid correlation for the model is noteworthy.

Model 6, seen in Figure 6, was the most interesting slice because it contained lipid pools, calcification, fibrous plaque and arterial wall.

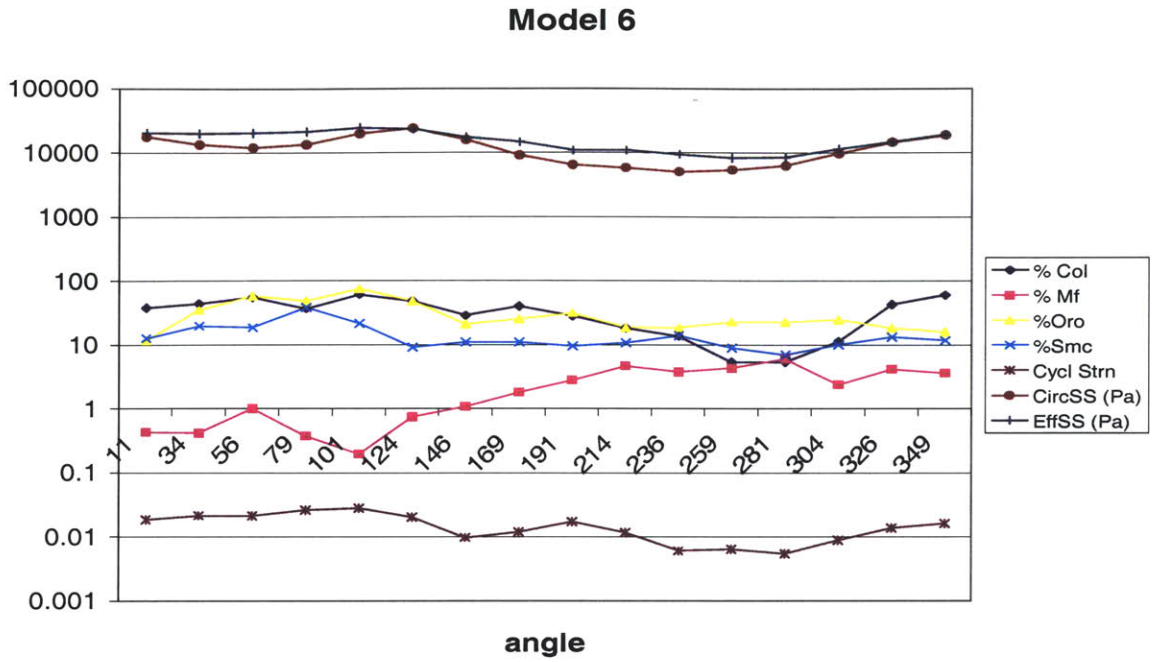

Figure 27: Circumferential Variation of % histology components and physiological variable for Model 6

Model 6 showed a positive correlation between Smooth Muscle Cells and CyclStrn / EffSS. This model also showed a positive correlation for Lipid vs CyclStrn due to the presence of extracellular lipid pools. Unlike Models 3 and 4 which showed a negative relationship between Collagen and CyclStrn / CircSS / EffSS, Model 6 exhibited a positive relationship, indicating contradictory relationship. A strong negative relationship was also found between Macrophage and CyclStrn / CircSS / EffSS.

3.4 Correlations

In all, 6 specimens were simulated using FEM and analyzed for correlations between the 4 histological markers (LIP, COL, SMC, MΦ) and the 3 physiological parameters, (CycS, CircSS, EffSS). This analysis produced a number of significant correlations. The correlations were run for each individual model using STATA, and the raw data can be viewed in Appendix B. The correlation analysis was run twice because

the two different measures of the histology were used. The first correlation was run using the absolute quantification of the histology (counting the number of pixels that represented a specific staining of the plaque). This rationale would be appropriate if the stimulus (the physiological parameters in this study) led to the addition of a particular component without otherwise changing the wall composition. A second measure of histology was conducted by "normalizing" the absolute quantification of each 22.5 degree segment of plaque by the intimal area of its respective sector. Normalization provided a measure of the fraction of total area within the segment stained for each of the individual components. This rationale would be better if remodeling of atherosclerotic plaque led to a breakdown of existing material and replacement by new material.

The correlations found in the absolute and normalized runs coincided for the results concerning macrophage. The correlations showed opposite trends for the relationships between smooth muscle cells and stress/strain. The normalized correlation showed a positive correlation between smooth muscle cells and stress/strain, while the absolute correlation showed a negative correlation. Both absolute and normalized correlations proved to be inconclusive for data concerning lipid and collagen.

3.4.1 Absolute Correlation

At first it seemed most appropriate to use the absolute correlations since the absolute histology values were thought to be more indicative of remodeling that occurs due to changes in stress/strain. Using the data for the absolute quantification of the histology and the stress/strain data from FEM analysis, the absolute correlations were run on STATA.

The absolute correlations showed a strong negative relationship between collagen and all three physiological markers (CycS, CircSS, EffSS). This indicated that an increase in stress and strain is related to a decrease in the amount of collagen present in the plaque. Macrophage and smooth muscle cells also showed this same negative correlation against stress and strain. Lipid also showed a negative correlation, however it was not strong enough to be able to draw any conclusions about the impact of stress and strain on the remodeling of those histology markers. This is because the lipid correlations were not very representative of the actual LIP vs CycStrn / CircSS / EffSS relationship seen in these specimens. The histological quantification of lipid included intracellular and extracellular lipid, whereas the modeling of lipid only included extracellular lipid (lipid pools) due to it's very different material properties.

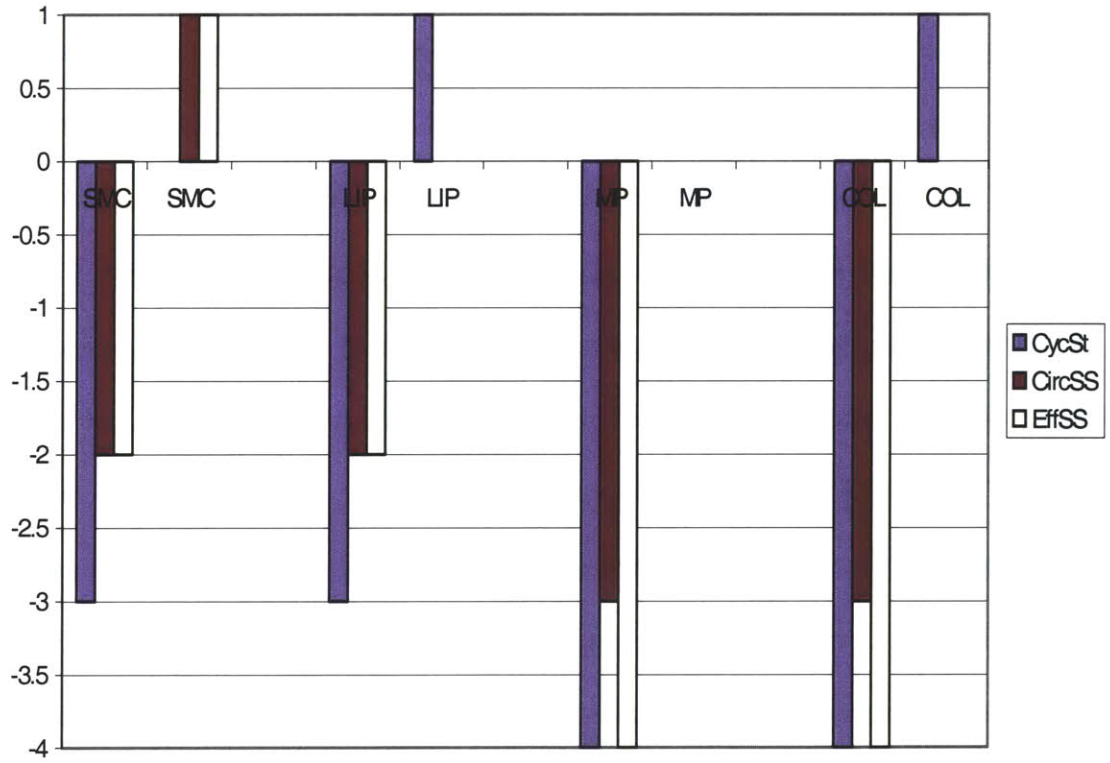

Figure 28: Number of Absolute Correlations for absolute quantification of histology

All the correlations using absolute quantification of histology were negative due to geometrical reasons. When examining the histology stainings, it can be seen that in the regions which have thicker walls, there will be more SMC, MP, LIP, and COL. As explained earlier thicker regions also experience low stress and strain since the thickness of the vessel is indirectly proportional to the stress in the vessel wall. Consequently, regions of low stress and strain always coincide with regions of high concentration of all four histological components, thus providing negative correlations for everything. Since this does not show proper insight into the atherosclerotic remodeling process, STATA was run again to find correlations between the normalized histology quantification and the physiological parameters.

3.4.2 Normalized Correlation

When normalizing each parameter, the absolute quantification for each sector was divided by the area of the sector. Due to the feasibility in the ability to consistently normalize these histological parameters, as well as it's more accurate description of the histology, it was decided that the normalized correlations would be a better indicator of the relationship between stress/strain and the remodeling of plaque composition.

Unlike what was seen in the absolute correlations, the normalized correlations showed that the relationship between Collagen and all three physiological markers (CycSt, CircSS, EffSS) as well as Lipid and the markers is inconclusive. A negative correlation could also be seen between macrophage and stress/strain, thereby agreeing with the absolute correlations. The major difference lay in the correlations of Smooth Muscle Cells and stress/strain. In the normalized correlations, SMC only exhibited a

positive correlation with the physiological markers, whereas the absolute correlations demonstrated a negative relationship.

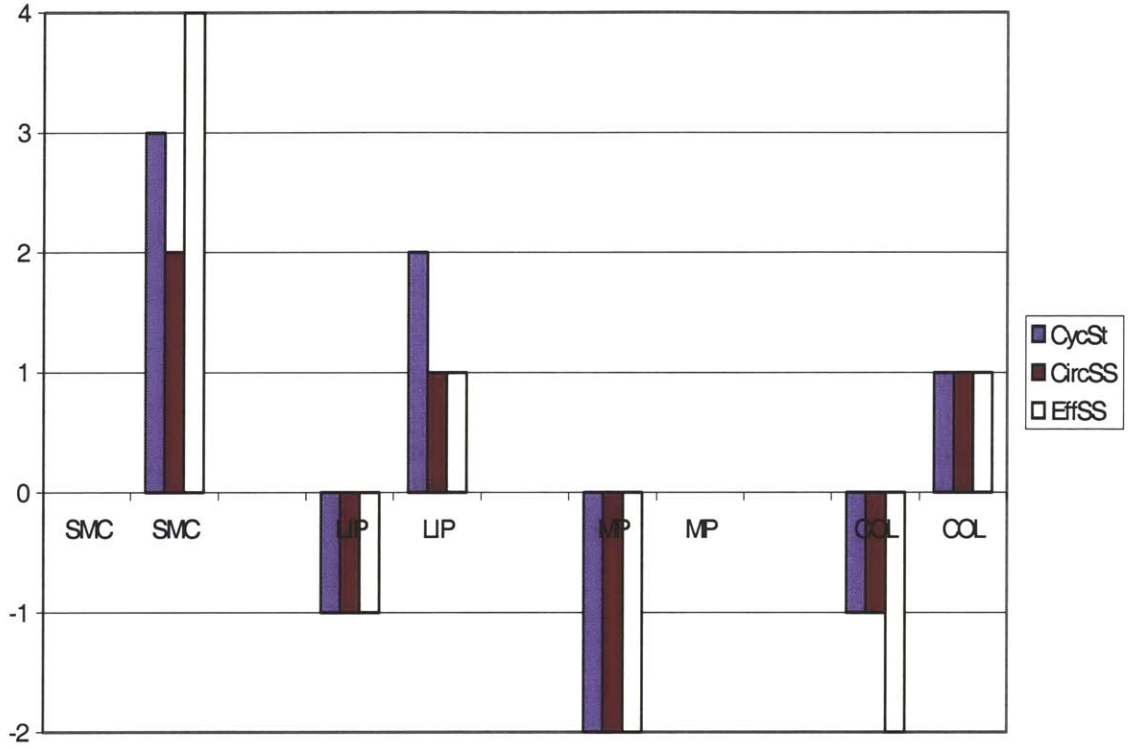

Figure 29: Number of Normalized Correlations for percent quantification of histology

3.4.3 Individual Model Correlations

Each model's correlation coefficients were compared across components and physiological variables (cyclic strain, circumferential stress, and effective stress). Since SMC and MP were the only components which were found to exhibit a meaningful correlation, those two were the only components considered in the following results.

3.4.3.1 (Absolute) Individual Model Correlations

The absolute correlations showed strong negative correlations for all four histology components (LIP, MP, COL, SMC) vs. CyclStrn / CircSS / EffSS. For a few

models, an interesting trend was noticed in the magnitude of the correlation coefficient. The Cyclic Strain exhibited a strong correlation between cyclic strain and the histology, and a weaker correlation between the stresses and the histology.

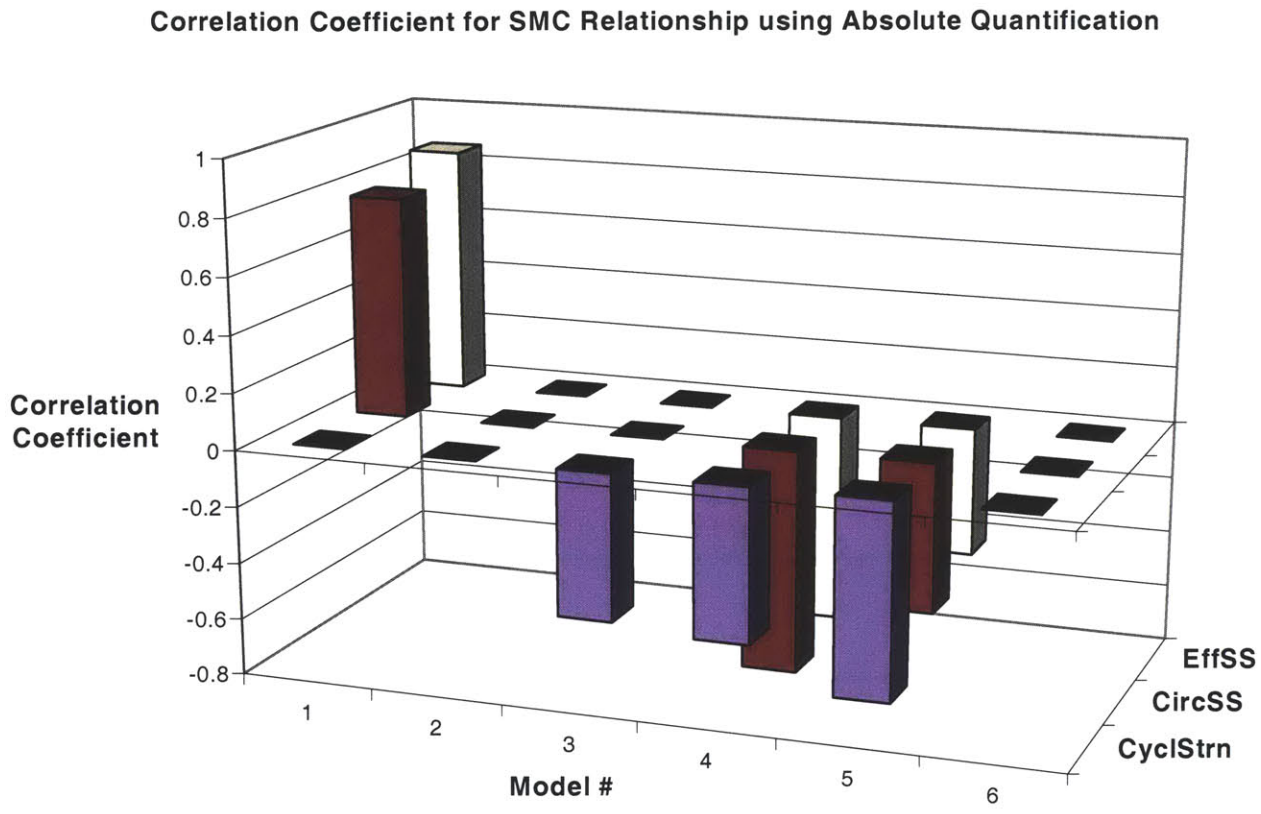

Figure 30: Absolute Correlation Coefficients for SMC found in all Models

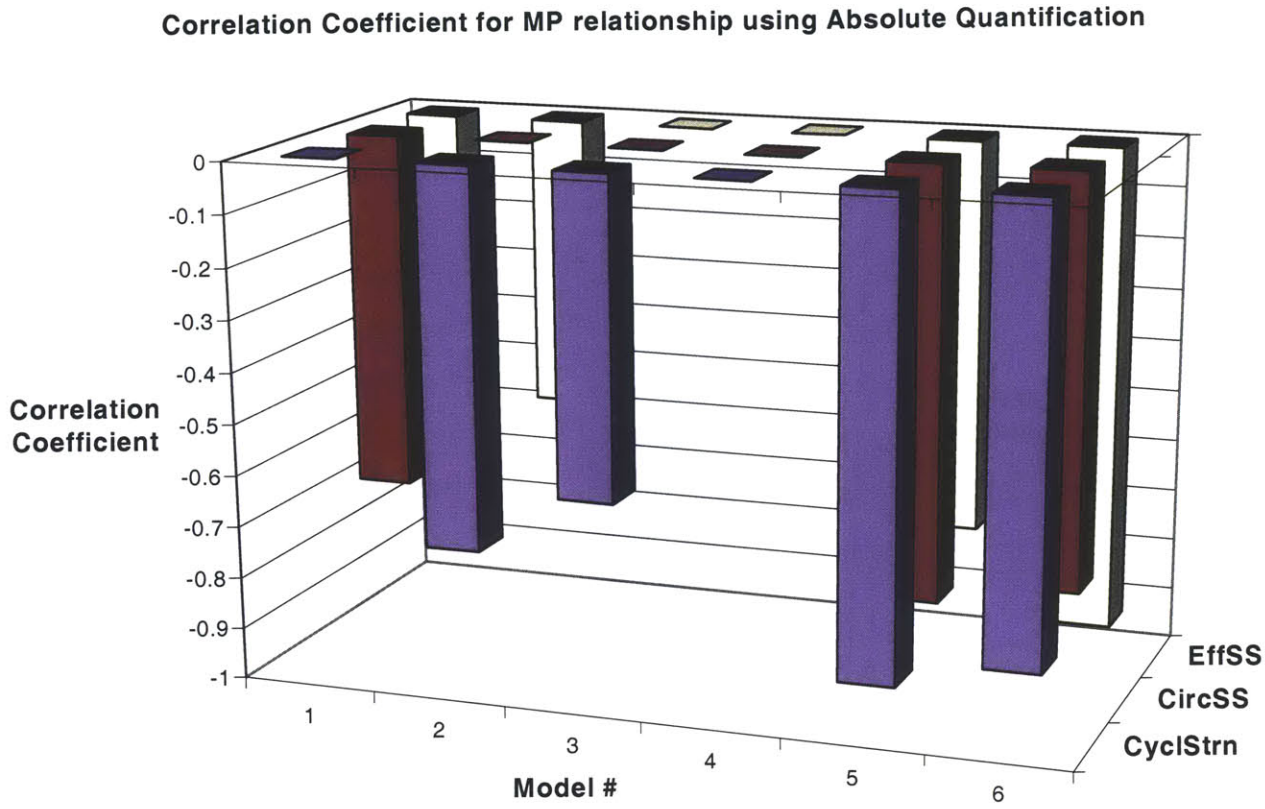

Figure 32: Absolute Correlation Coefficients for MP found in all Models

3.4.3.2 (Normalized) Individual Model Correlations

The normalized correlations were strongly negative for Macrophage vs CyclStrn / CircSS / EffSS and positive for Smooth Muscle Cells vs. CyclStrn / CircSS / EffSS. However, the relationships for Lipid and Collagen could not be determined due to differing relationships among the models.

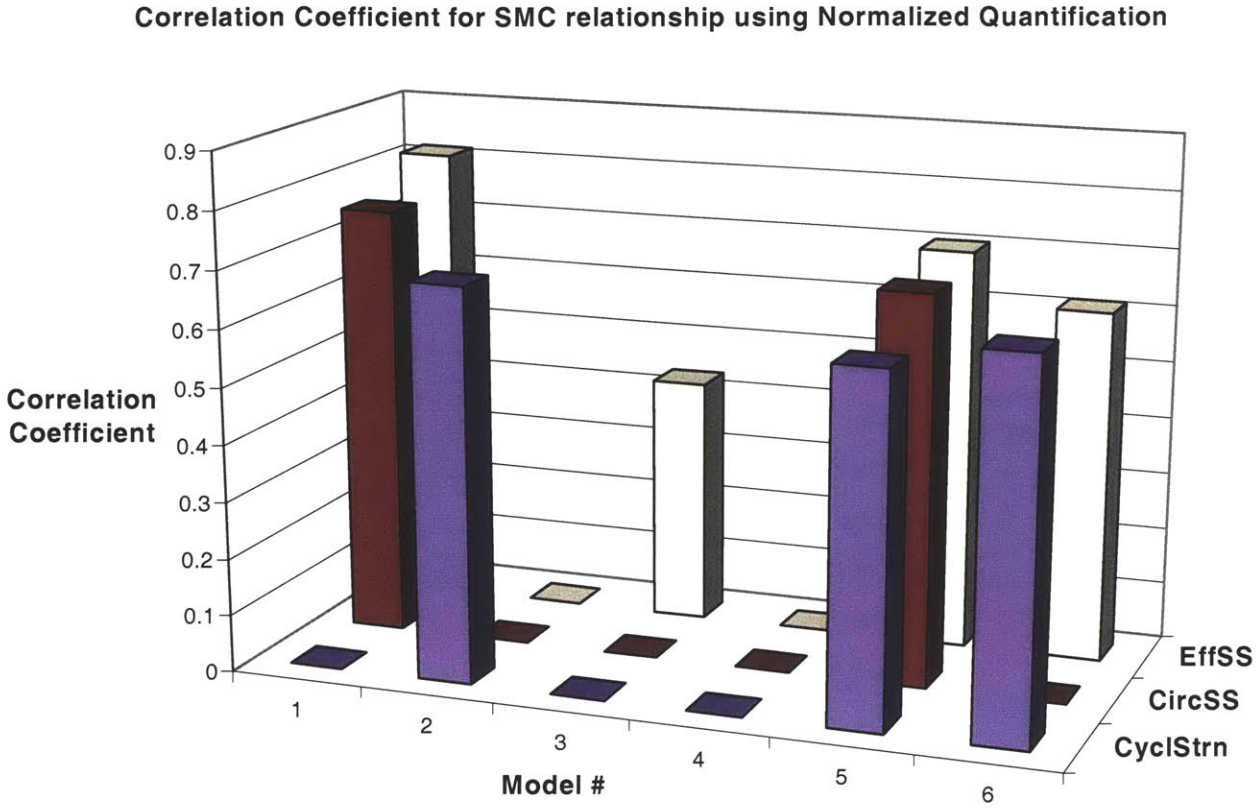

Figure 33: Normalized Correlation Coefficients for SMC found in all Models

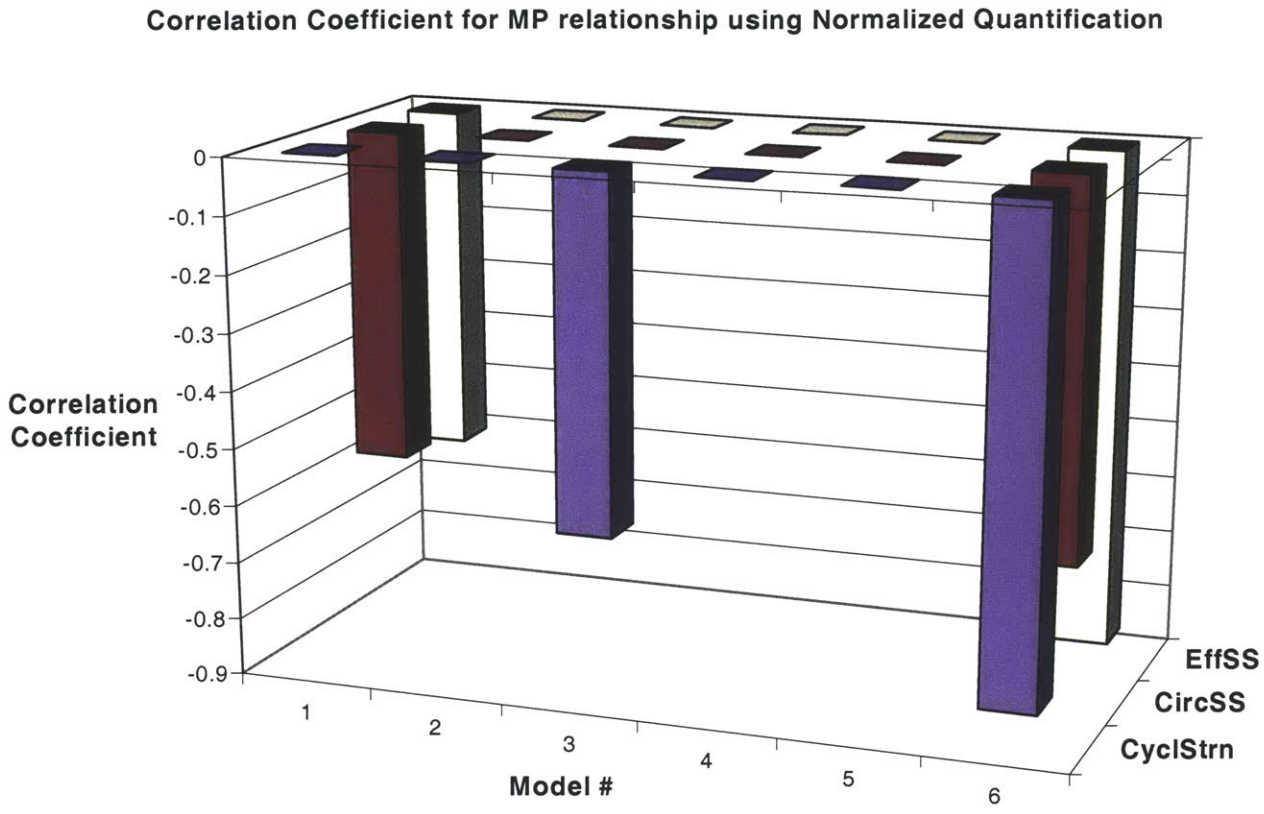

Figure 34: Normalized Correlation Coefficients for MP found in all Models

Unlike the absolute correlations, the normalized correlations did not exhibit the same trend of having the CyclStrn correlation coefficient stronger than the coefficient for CircSS/ EffSS. Also, the normalized correlations showed more conflicting trends in each of the four components. For example, in the correlation between Collagen vs. CyclStrn / CircSS / EffSS, Model 3 showed an entirely negative correlation, while Model 6 showed an entirely positive correlation. Similarly, the relationship between Lipid and CyclStrn / CircSS / EffSS was negative for model 5, yet positive for model 3. This most likely due to the fact that they both contained only intracellular lipid.

In Discussion, the stress/ strain distribution will be discussed as well as the trends seen between the histology and physiological markers. Discussion of the results which

were obtained with absolute quantification of histology will be omitted since it has already been established that these results are trivial.

4. Discussion

The purpose of this study is to see if there exists a relationship between physiological variables such as stress and strain, and plaque remodeling. Since the progression of atherosclerosis is currently under investigation, this research is instrumental for assessing the diagnosis and prognosis of atherosclerotic patients. By finding a relationship between stress/strain and histological remodeling, we are provided with better tools to evaluate the stages of atherosclerosis.

In this investigation we found a negative correlation between macrophage density and stress/strain. We also found a positive relationship between SMC and Cycl Str / EffSS / CircSS. The data were inconclusive in terms of relationships with either lipid or collagen.

4.1 Stress/ Strain Distribution

There were some common trends observed in the six models. The models containing lipid pools experienced the maximum cyclic strain inside the lipid pools whereas in the other models maximum cyclic strain occurred on the inner border of the plaque. This latter observation can be explained simply on the basis that the inner circumference undergoes higher strain than the outer. This is proven below in Figure 35. The models with lipid experienced maximum strain in the lipid pool since a lipid pool is significantly more compliant than the other three histological materials used for modeling.

Another trend seen in the cyclic strain plots related to the variation across the vessel wall. From the plots shown in the results sections, cyclic strain varied from 2-4 %

in most of the models. Although this seems to be a large variation, it can be proven that this is a reasonable gradient.

By analyzing a uniform thickness cylinder, we can estimate the theoretical strain gradient, as well as prove that the inner boundary is more strained than the outer boundary.

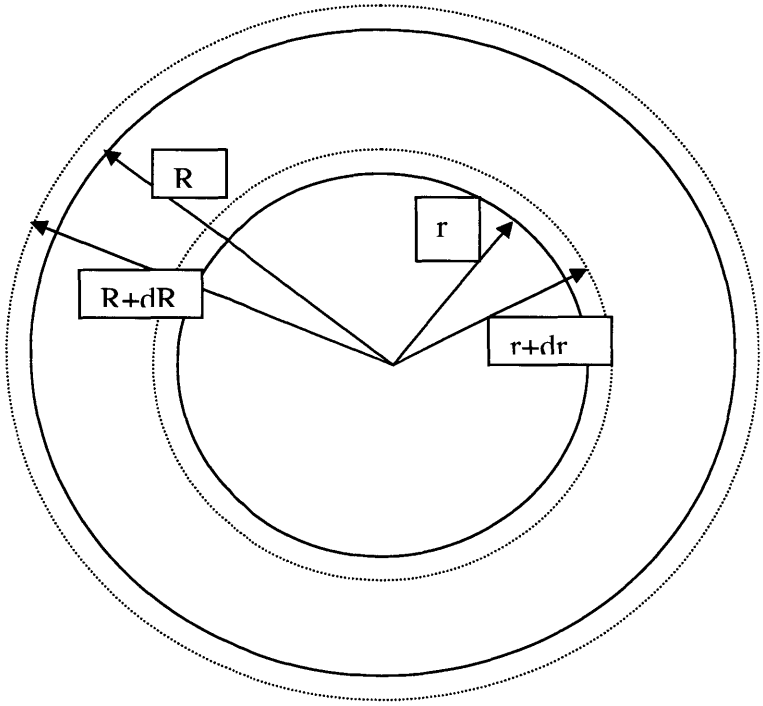

Figure 35: The displacement of an annulus by 'dr'

For an incompressible material under plane strain the wall area remains constant,

$$\pi R^2 - \pi r^2 = cons\tan t$$
$$R^2 - r^2 = (R + dR)^2 + (r + dr)^2$$
$$RdR = rdr$$
$$\varepsilon(outer) = \frac{dR}{R}, \varepsilon(inner) = \frac{dr}{r}$$

we obtain the result:

$$\varepsilon(outer) = \left(\frac{r}{R}\right)^2 \varepsilon(inner)$$

Since r is always smaller than R, the outer edge of the cylinder always experiences less strain than the inner edge. Further, this result can be used to estimate the strain which should be seen in the models. The thickness of the plaque is approximately 1 mm, with the inner radius being approximately 4 mm, and the outer radius being approximately 5mm. Using the above equation, we find that the strain in the outer wall can be up to 64% of the inner wall strain. Hence, a strain of 0.02 in the outer wall is not unreasonable when the inner wall is strained at 0.04. Note that this argument applies whether or not residual stress is taken into account.

The maximum effective and circumferential stress was between 200 kPa and 500 kPa, for the six models. Models 5 and 6 were the only models that showed a relatively low maximum effective and circumferential stress of approximately 200 kPa. This coincides with Huang et al. [9] findings that calcification seems to lower stress in the plaque due to its stiff material properties. The calcification is able to withstand a large amount of the wall stress, thereby reducing the stress in the fibrous plaque areas, especially proximal to the calcification. However, it raises questions regarding the theory that plaque rupture

occurs as a result of high stress levels, since in this study, vessels with relatively mild disease exhibited the highest levels of stress.

Note that according to Cheng et al. [8], the average pressure necessary for rupture is 300 kPa. In that study the specimens were modeled and inflated to an interluminal pressure of 110 mmHg. This measure was found by examining the maximum circumferential stress in specimens which had ruptured in vivo. While this study used an average interluminal pressure, our study used the patient specific systolic pressure to examine circumferential/effective stress. All the patients studied had elevated blood pressures, typical of many patients with arterial disease, ranging from 144 mmHg- 201 mmHg. This would account for the fact that several of the models (from models 1, 2, and 3) experienced stress higher that 300 kPa and had not ruptured yet. The critical level of stress for rupture, then, might be significantly higher than the 300 kPa value found previously.

4.2 Effect of Residual Strain

The effect of incorporating residual strain was also analyzed to see if it is necessary in simulating in vivo conditions. Three examples (Models 1, 2 and 3) were run in order to investigate the effects of residual strain in different types of specimen.

Model 1 contained a lipid pool, arterial wall, and fibrous plaque, whereas Models 2 and 3 contained only arterial wall and fibrous plaque. The model with lipid (Model 1) did not show much of a difference in the cyclic strain profile whether or not residual strain was included (see Figure 19). Models 2&3 (without lipid) also showed little change in maximum cyclic strain (~4.6%) between the simulations with and without residual strain. The regions of highest strain were notably in the inner fibrous plaque region of the

model, near the shoulder regions of the plaque. In the simulations that incorporated residual strains, large cyclic strains were also visible in the shoulder regions. In both simulations, the point of least cyclic strain lay on the outer edge of the artery for the reasons described above.

Unlike cyclic strain, the effective and circumferential stress profiles, did differ between the simulations with and without residual stress. The stress gradient across the thickness of the wall was much higher when residual strain was not incorporated since the presence of residual stress reduces the stress gradient across the thickness of the artery. Consequently the stress gradients were larger in the simulations without residual stress, causing both the maximum stress to be higher and the minimum to be lower in this case.

This result has important implications in the modeling of arteries or any pressure vessel with residual stresses. In previous studies such as Cheng et al. [8], it was instrumental to find the maximum stress values of the model in order to determine a reasonable indicator of the stress at rupture. By not including residual stress in the model, there is the potential to find an inaccurate representation of the rupture stress. Most likely this reported stress will be higher than what was actually occurring in vivo. Consequently, it is important to incorporate residual stress when examining these arterial models.

4.3 Circumferential Variation

The circumferential variation of histological and physiological parameters was analyzed for each model. Previous work by Kaazempur- Mofrad et al, [19] showed that correlations could be identified between the histological markers in the arterial wall and the hemodynamic factors, such as mean wall shear stress or the temporal gradient in shear. High shear stress can be atheroprotective whereas low shear stress can cause an area to be more prone to the progression of atherosclerosis. The present study focused, instead, on the stresses acting inside the wall.

Model 1 was located approximately 7 mm below the carotid bifurcation in a region of relatively healthy area of the carotid artery. This area was not heavily stenosed, suggesting low wall shear stress and laminar flow. The correlations found for this model included a positive relationship between SMC and CircSS/ EffSS, a positive relationship between LIP and CycStrn, and a negative relationship between MP and CircSS /EffSS. The positive relationship between LIP and CycStrn can immediately be seen by referring to the Model 1 Bandplot of Cyclic Strain in Results. The lipid pool region showed the highest cyclic strain in the entire model. Further, since this specimen is located in a region of low shear stress, it may be have been easier for the infiltration of monocytes, causing a higher macrophage concentration in the lipid region which exhibits low CircSS /EffSS.

Models 2-5 came from the same carotid artery. Models 2 and 3 were located significantly below the carotid bifurcation and were again in areas of mild disease. They showed a positive correlation between SMC and CycStrn, and between LIP and EffSS. They also exhibited a negative correlation between MP and CycStrn as well as between

COL and CycStrn / CircSS / EffSS. These models were located so low on the carotid artery, they were in relatively healthy sections of the artery with uniform fibrous plaque and no lipid pools or calcification. Consequently, there was only a small amount of MP in the models (especially Model 3), causing the negative correlation of low significance. The negative correlation between COL and CycStrn / CircSS / EffSS, seemed to be reasonable due to the inflammatory process of atherosclerosis. One possible explanation for this negative relationship is that high cyclic strain or stress might have induced the cells locally to produce more MMPs (as found in the studies of Lee et. al [7]) , thereby enzymatically breaking down the collagen and causing it to become depleted. This would lead to low collagen content in areas of increased CycStrn / CircSS / EffSS. This relationship will be examined in further detail when discussing the Circumferential Variation in Model 6.

Model 4 was located nearer to the carotid bifurcation than Models 2 and 3. It was slightly more diseased and therefore experienced more shear stress due to the narrowing of the artery in that region. This model did not have any lipid pools or calcification and only demonstrated a negative correlation between COL and CycStrn / EffSS due to the relatively uniform distribution of all three components.

Model 5 was located a few millimeters distal to the carotid bifurcation, on the internal carotid artery. In addition to fibrous plaque and normal arterial wall, it had one large area of calcification. It showed a positive relationship between SMC and CycStrn / CircSS / EffSS, and a negative relationship between LIP and CycStrn / CircSS / EffSS. This model was in a highly stenosed area of the artery and most likely experienced a very high wall shear stress which likely inhibited the entry of monocytes into the plaque. The

negative LIP correlation which is contrary to the result found in Models 1, 3, and 6 could be explained by the large circumferential variation of intracellular lipid. As mentioned in Results, the quantification of lipid included intracellular and extracellular, whereas the modeling of lipid included only extracellular. This discrepancy could have caused these inconsistent lipid correlations.

Model 6 was located in a highly stenosed region of the internal carotid artery. It was unique in that it contained lipid pools and calcification in addition to arterial wall and fibrous plaque. Huang et al's study [9] showed that lipid increases the stress near the lipid pool, whereas calcification lessens the stress proximal to areas of calcification, thereby increasing the stability of the plaque. This specimen contained 6 areas of calcification and 2 lipid pools, with the lipid pools closer to the outer boundary of the plaque and the calcification closer to the lumen. Due to its proximity to the lumen, the calcification effect dominated the lipid effect and seemed to produce a relatively low maximum effective and circumferential stress of approximately 250 kPa. The odd results though, lay in the correlation with lipid. One would expect there to have been a region of high stress surrounding a lipid pool due to the lipid's compliant nature, however no correlation was found between lipid and either stress indicator (CircSS/EffSS). This could be due to the complexity of the composition of the plaque. This specimen may not have exhibited the usual remodeling process due to the proximity of two very different materials, lipid and calcification. Model 6 also exhibited the expected negative correlation between COL and CycStrn / CircSS / EffSS. This agrees with the concept of collagen being the primary component of the extracellular matrix of fibrous plaque.

4.4 Correlations (Percentage Only)

After reviewing the individual correlations of all 6 models, it was determined if a significant relationship was found for each histological component. Of the four histological components studied, it was determined that only two (SMC, MP) showed significant correlations. LIP and COL both had inconclusive results due to positive and negative correlations found in different models.

It has been hypothesized that the region near lipid pools are areas of high stress and contribute to the vulnerability of the plaque [6]. This can be explained due to the effective thinning of the wall locally, as well as the stress concentrations near the edge of the lipid pool. However no significant correlation concerning lipid and stress was found in this investigation, except for Models 1 and 6, (both of which contained at least one lipid pool). Both models did though show a positive relationship between cyclic strain and lipid. The lack of lipid correlations with stress can be explained, at least in part, by the method in which lipid was quantified. All 4 histological markers were quantified according to the area of the specimen which was stained. For lipid, this included intracellular and extracellular lipid. In the FEM models, only lipid pools were considered in order to assign the material properties which characterize it as a very soft region. Due to the inconsistency in the definition of lipid, it is plausible to see that no conclusive correlation was found for lipid.

The positive correlation found with smooth muscle cells and CycStrn / CircSS/EffSS can most likely be explained by the large stresses near the lumen region. The high stress in the fibrous cap area may cause the remodeling of the plaque, which involves the formation of extracellular matrix which is rich in collagen as well as smooth

muscle cells. According to Ross [13], at sites where cell injury and necrosis occur, the damaged smooth muscle cells could play a principal role in the fibroproliferative component in the process of this disease. The smooth muscle cells in the fibrous cap region could be injured due to the large amount of effective and circumferential stress being experienced, and consequently these smooth muscle cells experience a change in phenotype and begin secreting collagen, elastic fibers, proteoglycans, as well as more smooth muscle cells.

A slight negative correlation was found between macrophage and CycStrn/CircSS/EffSS. Macrophages are monocytes which ingest low density lipoprotein particles and become foam cells. The macrophages are usually located in shoulder areas of the plaque and release enzymes such as matrix metalloproteinase (MMP) which degrade and weaken the fibrous cap. This chemical pathway can be seen in the observation of Lee et. al who found a significant positive correlation between circumferential stress and the presence of MMP [7]. This finding contradicts the work of Lendon et. al [22] who observed that atherosclerotic plaque caps are locally weakened when macrophage density is increased. It seems that the plaque experiences a decrease in stress in regions that contain macrophages.

The negative correlation found in this current study suggests that areas of low CycStrn/CircSS/EffSS, such as thicker areas of the artery are more prone to attracting macrophages. In accordance with Lee et al., the macrophages could proceed to use the MMP to break down the plaque thereby causing high stress. Hence, the macrophage correlation seems to depend on the stage of atherosclerosis of each specimen.

This leads into the explanation for why inconclusive results were found for the relationship between collagen and CyclStrn / CircSS / EffSS. Approximately equal number of correlations showed positive and negative relationships between Collagen and CyclStrn / CircSS / EffSS. Model 3 showed a completely negative trend, while Model 6 showed a completely positive trend. A loss in collagen in areas of increased stress and strain can be explained due to MMP, discussed earlier. High stress and strain induce macrophage migration and secretion of MMP which degrade collagen and extracellular matrix thereby weakening the atherosclerotic plaque and leading to low levels of collagen.

However, high levels of collagen can be explained by the previously mentioned fibroproliferative process whereby high stress/ strain triggers smooth muscle cells to secrete collagen and proteoglycans, consequently strengthening the plaque in order to compensate for the increased stress/strain [1]. Consequently, both of these biological mechanisms can explain the increase or decrease in collagen due to increased stress and strain.

Finally, as mentioned previously in the results, it was interesting to note the trend that cyclic strain often had a stronger correlation coefficient than circumferential or effective stress. This trend follows the evidence that it is the cyclic variation that triggers remodeling of the plaque. Seliktar et al. showed that dynamic mechanical conditioning (in the form of cyclic strain) during tissue culture leads to an improvement in the properties of tissue-engineered blood vessel in terms of mechanical strength and histological organization [23]. Plaque composition seems to be more sensitive to changes in cyclic strain due the constant fluctuation of strain. This is unlike changes in

circumferential/effective stress, which causes cells to respond in the beginning, but return to their initial configuration soon after the transient response dies down. Since the cyclic strain is the only physiological indicator which incorporates the variation along a cycle, it is expected to show the strongest correlation. The circumferential and effective stress both show approximately the same degree of correlation with the histology markers.

5. Conclusion

From this investigation, it can be concluded that smooth muscle cell and macrophage content are reasonable indicators for detecting areas of high stress. An increase in smooth muscle cell content and decrease in macrophage content indicate areas of high stress and strain. This is most likely due to the fibroproliferative remodeling response of atherosclerotic plaque. It was also found that regions of high stress and strain do not imply anything about collagen content due to the nature of the remodeling process. We can also confirm previous studies that show that lipid pools increase the stress felt in the plaque, whereas calcification decreases the stress experienced in the plaque. Further, this investigation also supports the theory that the thickness of the fibrous cap plays an important role in the effective and circumferential stress in the plaque.

This study also supports the theory that it is essential to include the effects of residual stress. Incorporation of residual stress changes the maximum effective and circumferential stress by a significant amount, despite only small changes in cyclic strain.

Areas of high effective stress, circumferential stress, and cyclic strain, are important indicators of vulnerability of the plaque. By examining different relationships between the histology of the plaque and the stress in the artery, we hope to be able to detect plaque vulnerability with a more noninvasive approach, and at an earlier time in the progression of the disease.

References:

1. Lilly, Pathophysiology of Heart Disease
2. http://medweb.bham.ac.uk/http/depts/path/Teaching/foundat/athero/athero4.htm
3. Berne and Levy, Physiology, Fourth Edition
4. www.adam.com
5. Richardson PD, Davies MJ, Born GV. Influence of plaque configuration and stress distribution on fissuring of coronary atherosclerotic plaques. *Lancet.* 1989; 2:941-944.
6. Loree HM, Kamm RD, Stringfellow RG, Lee RT. Effects of Fibrous Cap Thickness on Peak Circumferential Stress in Model Atherosclerotic Vessels. *Circulation Research.* 1992; 71:850-858.
7. Lee RT, Shoen FJ, Loree HM, Lark MW, Libby P. Circumferential Stress and Matrix Metalloproteinase 1 in Human Coronary Atherosclerosis. Implication for Plaque Rupture. *Arteriosclerosis Thrombosis and Vascular Biology*, 1996;16: 1070-1073.
8. Cheng GC, Loree HM, Kamm RD, et al. Distribution of Circumferential Stress in Ruptured and Stable Atherosclerotic Lesions: A Structural Analysis with Histopathological Correlation. *Circulation,* 1993; 87: 1179-1187.
9. Huang H, Virmani R, Younis H, Burke AP, Kamm RD, Lee RT. The Impact of Calcification on the Biomechanical Stability of Atherosclerotic Plaques. *Circulation*, 2001; 103:1051-1056.
10. Holzapfel GA, Stadler M, Schulze-Bauer CAJ. A Layer Specific Three-Dimensional Model for the Simulation of Balloon Angioplasty using Magnetic Resonance Imaging and Mechanical Testing. *Annals of Biomedical Engineering*, 2002;30:753-767.
11. Zhao SZ, Ariff B, Long Q, Hughes AD, Thom SA, Stanton AV, Xu XY. Inter-Individual Variations in Wall Shear Stress and Mechanical Stress Distributions at the Carotid Artery Bifurcation of Healthy Humans. *Journal of Biomechanics*, 2002; 35:1367-1377.
12. Delfino A, Stergiopuos N, Moore JE, Meister JJ. Residual Strain Effects on the Stress Field in a Thick Wall Finite Element Model of the Human Carotid Bifurcation. *Journal of Biomechanics*, 1997; 30:8:777-786.
13. Ross R. Atherosclerosis – An Inflammatory Disease. *New England Journal of Medicine*, 1999; 340:2:115-126.
14. Delfino A. Analysis of stress field in a model of the human carotid bifurcation. *Physics*. Lausanne: Ecole Polytechnique Federale De Lausanne; 1996.
15. Loree HM, Grodzinsky AJ, Park SY, et al. Static Circumferential Tangential Modulus of Human Atherosclerotic Tissue. *Journal of Biomechanics.* 1994; 27:195-204.
16. Loree HM, Tobias BJ, Gibson LJ, et al. Mechanical Properties of Model Atheroslcerotic Lesion Lipid Pools. *Arteriosclerosis Thrombosis and Vascular Biology*. 1994; 14:230-234.
17. ADINA R&D, Inc. *Theory and Modeling Guide for ADINA.* Watertown, Mass: ADINA; 2000.
18. Humphrey JD. Critical Reviews in Biomedical Engineering, *Mechanics of the Arterial Wall: Review and Directions,* pp25-26.

19. Kaazempur-Mofrad MR, Younis HF, Isasi AG, et. al. Diseased Carotid Bifurcation Fluid Mechanics Based on in vivo Magnetic Resonance Images: Relationship of Shear Stress and Inflammation. Submitted to the *Journal of Biomechanics.*
20. Rosner BA, Regression and Correlation Methods; Fundamentals of Biostatistics, PWS Publishers, Boston, MA 419-424, 1986.
21. Bickford WA, Thin Walled Pressure Vessels; Mechanics of Solids, Irwin Publishers, USA, 606-610, 1993.
22. Lendon CL, Davies MJ, Born GVR, Richardson PD. Atherosclerotic Plaque Caps are Locally Weakened when Macrophages Density is Increased. *Atherosclerosis.* 1991; 87: 87-90.
23. Seliktar D, Black RA, Vito RP, Nerem RM. Dynamic mechanical conditioning of collagen-gel blood vessel constructs induces remodeling in vitro. *Annals of Biomedical Engineering.* 2000;28 (4): 351-62.

Appendix A

p3slice1

Slice 1	% Col	% Mf	%Lip	%Smc	angle	Col	Mf	Lip	Smc	Cycl Strn	CircSS	EffSS
11.25	2.877598	4.51429	15.81316	13.06762	11.25	0.14992	0.23519	0.82385	0.68081	0.041607	47345.97	52009.34
33.75	15.79858	3.965133	10.807	8.598885	33.75	1.3974	0.35072	0.95589	0.76058	0.039982	46244.97	51112.66
56.25	22.60547	6.097852	10.50293	8.434961	56.25	2.3148	0.62442	1.0755	0.86374	0.038602	53119.33	54738.1
78.75	7.204458	0.907467	3.286852	11.73077	78.75	0.89537	0.11278	0.40849	1.4579	0.036142	56153.16	56884
101.25	1.162396	0.849927	2.774718	9.974555	101.25	0.12791	0.093526	0.30533	1.0976	0.03142	59623.73	57882.11
123.75	12.60552	7.514135	3.626101	2.550033	123.75	1.9173	1.1429	0.55153	0.38786	0.026066	55772.7	51035.09
146.25	7.984092	11.22946	4.549831	1.760535	146.25	1.5157	2.1318	0.86374	0.33422	0.031383	42024.87	48975.51
168.75	8.041664	13.62782	4.357997	1.66937	168.75	1.3781	2.3354	0.74683	0.28608	0.042961	38389.83	39268.7
191.25	9.073428	10.5413	2.701225	1.891809	191.25	1.3259	1.5404	0.39473	0.27645	0.036496	32131.99	39999.53
213.75	9.961433	8.859204	3.802655	5.152918	213.75	0.9944	0.88437	0.3796	0.51439	0.032891	37798.07	42515.47
236.25	25.17495	15.75629	6.321454	9.180428	236.25	2.18	1.3644	0.5474	0.79497	0.034188	55654.03	55073.31
258.75	28.05405	11.48872	1.90513	1.846972	258.75	2.6531	1.0865	0.18017	0.17467	0.031197	45762.03	46580.84
281.25	18.17132	12.82877	2.093972	2.057835	281.25	2.0768	1.4662	0.23932	0.23519	0.030935	42785.83	43375.03
303.75	29.84485	7.765193	2.714702	6.691912	303.75	2.6008	0.67669	0.23657	0.58316	0.032797	44899.64	45310.77
326.25	14.52335	3.874288	3.711913	13.38746	326.25	0.98477	0.2627	0.25169	0.90775	0.032776	53661.8	51803.23
348.75	0.533675	6.175422	9.606068	32.19822	348.75	0.028883	0.33422	0.51989	1.7426	0.040249	63568.41	62324.5

p1slice2

Slice 2	% Col	% Mf	%Lip	%Smc	Slice 2	Col	Mf	Lip	Smc	Cycl Strn	CircSS	EffSS
11.25	22.85001	1.668783	4.877518	34.25529	11.25	0.26995	0.019715	0.057623	0.404692	0.047154	80283.76	72434.1
33.75	8.064611	3.8979	5.376407	31.1832	33.75	0.090993	0.04398	0.060662	0.35184	0.047153	69462.21	67159.85
56.25	37.88591	2.834986	6.35756	22.90489	56.25	0.6688	0.050046	0.11223	0.40434	0.050203	60739.17	64984.72
78.75	57.66069	1.780892	6.149159	22.10999	78.75	2.6024	0.080377	0.27753	0.99789	0.050471	51493.54	62135.08
101.25	42.71648	0.36421	4.708728	47.89351	101.25	2.4902	0.021232	0.2745	2.792	0.05062	41597.45	56213.95
123.75	15.30918	1.031774	6.302105	38.14655	123.75	0.83259	0.056113	0.34274	2.0746	0.050262	46932.97	60216.21
146.25	57.38299	1.025437	5.947503	26.60013	146.25	4.2433	0.075828	0.4398	1.967	0.041792	62298.58	66532.73
168.75	59.2558	1.588033	5.977711	16.29993	168.75	7.9225	0.21232	0.79922	2.1793	0.037914	60012.67	58063.56
191.25	48.00905	0.862655	2.182715	10.58118	191.25	7.005	0.12587	0.31848	1.5439	0.035578	45188.42	43843.73
213.75	43.44171	5.729222	10.49391	11.57407	213.75	3.4153	0.45042	0.82501	0.90993	0.035407	38620.63	38932.8
236.25	34.16713	3.741896	4.696684	14.50304	236.25	2.0079	0.2199	0.27601	0.8523	0.041578	45626.54	48965.67
258.75	15.75042	1.482405	2.779497	32.92062	258.75	0.77344	0.072795	0.13649	1.6166	0.04471	47125.14	56325.76
281.25	29.399	1.210738	4.729436	39.12132	281.25	1.1784	0.04853	0.18957	1.5681	0.046661	44284.2	56574.14
303.75	25.10271	1.471828	1.880682	27.88322	303.75	0.46558	0.027298	0.034881	0.51715	0.050062	48447.42	60122.98
326.25	35.39569	1.364853	3.275695	37.39725	326.25	0.58994	0.022748	0.054596	0.6233	0.052337	58708.49	66002.36
348.75	28.9414	1.501665	2.457287	36.8593	348.75	0.64302	0.033364	0.054596	0.81894	0.051288	74940.46	74391.92

p1slice1

Slice 3	% Col	% Mf	%Lip	%Smc	Slice 3	Col	Mf	Lip	Smc	Cycl Strn	CircSS	EffSS
11.25	4.932524	0	0.639272	25.54126	11.25	0.10161	0	0.013169	0.52615	0.052535	53726.09	54346.29
33.75	1.920911	0	1.253697	17.34195	33.75	0.051563	0	0.033653	0.46551	0.053328	55419.66	55254.46
56.25	1.17132	0	0.75339	11.93861	56.25	0.040947	0	0.026337	0.41735	0.053318	60669.57	59058.06
78.75	5.451553	0	0.648911	24.18944	78.75	0.23355	0	0.0278	1.0363	0.052174	56793.93	57053.69
101.25	5.744533	0	0.862725	28.26615	101.25	0.32151	0	0.048285	1.582	0.049965	56911.97	56377.76
123.75	4.910922	0.034706	1.490017	28.24532	123.75	0.42919	0.003033	0.13022	2.4685	0.046485	55613.77	55361.97
146.25	6.90698	0	1.514509	25.19925	146.25	0.40037	0	0.08779	1.4607	0.039522	65139.1	60651.77
168.75	21.3619	0.016664	0.400813	20.40049	168.75	1.9442	0.001517	0.036479	1.8567	0.038116	56501.88	52928.22
191.25	34.74385	0.127542	0.666522	11.64973	191.25	4.9576	0.018199	0.095106	1.6623	0.037435	43914.87	42617.36
213.75	32.06483	0.222015	0.358683	8.330429	213.75	4.5997	0.031848	0.051453	1.195	0.036466	37567.39	38211.91
236.25	23.75585	0	0.857436	5.234426	236.25	1.3194	0	0.047622	0.29072	0.040359	36333.22	38832.2
258.75	15.64059	0	0.696987	21.4529	258.75	0.65667	0	0.029263	0.9007	0.046172	53119.05	51358.4
281.25	12.32565	0	0.522268	25.85722	281.25	0.4489	0	0.019021	0.94172	0.046447	53596.18	52383.2
303.75	19.63979	0	0.470583	21.26201	303.75	0.916	0	0.021948	0.99166	0.045588	52967.58	51944.15
326.25	15.42837	0	0.519674	29.86529	326.25	0.60814	0	0.020484	1.1772	0.049904	52381.33	52462.3
348.75	2.189557	0	0.528124	32.4033	348.75	0.036397	0	0.008779	0.53864	0.051559	54334.79	54409.39

p1slice3

Slice 4	% Col	% Mf	%Lip	%Smc	Slice 4	Col	Mf	Lip	Smc	Cycl Strn	CircSS	EffSS
11.25	24.2553	0.226687	0.939122	16.02977	11.25	1.1359	0.010616	0.04398	0.75069	0.052585	61696.1	54648.82
33.75	52.13732	0.58198	1.682656	14.29632	33.75	6.2497	0.069762	0.2017	1.7137	0.04418	43908.01	38590.1
56.25	65.84519	0.05946	1.88574	10.65195	56.25	11.756	0.010616	0.33668	1.9018	0.036092	35889.76	30437.66
78.75	62.47097	0.128862	5.927604	14.19192	78.75	11.028	0.022748	1.0464	2.5053	0.030361	33416.25	27277.03
101.25	54.70473	0.579413	4.155169	13.35116	101.25	10.023	0.10616	0.76131	2.4462	0.031558	32608.11	27514.42
123.75	31.8338	1.418159	11.95915	16.5254	123.75	4.7999	0.21383	1.8032	2.4917	0.032985	30369.88	28119.06
146.25	46.98316	2.11755	12.01676	16.53024	146.25	5.3838	0.24265	1.377	1.8942	0.03414	37977.29	33404.06
168.75	58.36713	1.744096	14.01896	11.01045	168.75	6.6486	0.19867	1.5969	1.2542	0.040806	48956.37	42513.54
191.25	43.70224	1.837906	16.32469	7.811227	191.25	5.1927	0.21838	1.9397	0.92813	0.041202	45640.31	39833.86
213.75	38.62062	0.346668	3.527252	16.81334	213.75	5.4065	0.04853	0.49378	2.3537	0.038516	39464	34511.22
236.25	41.67658	0.138726	1.259	0.951258	236.25	6.3786	0.021232	0.19269	0.14559	0.030325	38547.07	30711.07
258.75	46.09316	0.194427	1.309145	16.73419	258.75	5.3929	0.022748	0.15317	1.9579	0.030414	31738.75	26521.13
281.25	30.02482	1.949353	2.980025	29.46487	281.25	2.0322	0.13194	0.2017	1.9943	0.036334	38276.4	31251.29
303.75	36.13983	0.251404	3.739768	31.70939	303.75	1.744	0.012132	0.18047	1.5302	0.049524	52620.02	44457.75
326.25	34.69457	0.375046	1.969055	26.8168	326.25	1.1223	0.012132	0.063695	0.86747	0.056321	59854.16	53139.94
348.75	23.79737	0.103466	1.552004	14.22651	348.75	0.69762	0.003033	0.045497	0.41705	0.054885	69391.24	61268.66

p1slice5

Slice 5	% Col	% Mf	%Lip	%Smc	Slice 5	Col	Mf	Lip	Smc	Cycl Strn	CircSS	EffSS
11.25	44.40002	0.225054	2.330866	11.02772	11.25	5.1729	0.02622	0.271562	1.284803	0.032084	39370.64	40509.46
33.75	15.8671	0.131616	3.319591	11.33365	33.75	2.0321	0.016856	0.42514	1.4515	0.032526	35635.76	36981.71
56.25	21.95132	0.305784	10.83218	6.421433	56.25	4.4368	0.061805	2.1894	1.2979	0.025294	23984.42	26482.75
78.75	28.41779	0.200542	12.75187	2.43599	78.75	9.0235	0.063678	4.0491	0.7735	0.017948	15223.53	17710.4
101.25	28.69985	0.377471	4.338089	4.679442	101.25	8.971	0.11799	1.356	1.4627	0.011902	10764.41	13970.96
123.75	29.76473	0.195951	10.48609	3.447574	123.75	10.526	0.069296	3.7083	1.2192	0.011559	10451.42	12939.27
146.25	33.37996	0.119089	6.109433	3.245159	146.25	10.499	0.037457	1.9216	1.0207	0.014678	10795	13636.51
168.75	48.57978	0.287072	4.288116	5.884945	168.75	10.142	0.059932	0.89523	1.2286	0.017865	15053.25	17687.9
191.25	47.71778	0.422524	0.641329	7.101084	191.25	6.5569	0.058059	0.088125	0.97576	0.020497	22029.65	23793.16
213.75	60.99799	0.121185	0.605936	12.80547	213.75	5.6561	0.011237	0.056186	1.1874	0.026127	29141.97	30478.64
236.25	46.91692	0.173085	0.405205	6.164926	236.25	3.0359	0.0112	0.02622	0.39892	0.033809	34806.27	36258.93
258.75	39.72976	0.340137	0.680288	9.932077	258.75	1.0938	0.009364	0.018729	0.27344	0.037651	40472.41	40429.15
281.25	74.92516	0.101938	1.732923	6.626027	281.25	1.3766	0.001873	0.031839	0.12174	0.039329	40244.29	39309.06
303.75	30.46269	0.090665	1.541288	9.418852	303.75	0.62928	0.001873	0.031839	0.194569	0.041499	39200.66	39757.34
326.25	68.09474	0.476183	3.095181	7.142803	326.25	0.53564	0.003746	0.024347	0.056186	0.040356	35868.09	38050.88
348.75	19.0676	2.057643	2.7435	5.898557	348.75	0.26033	0.028093	0.037457	0.080533	0.037513	37183.12	39716.42

p2slice4

Slice6	% Col	% Mf	%Lip	%Smc	Slice 6	Col	Mf	Lip	Smc	Cycl Strn	CircSS	EffSS
11.25	38.13842	0.430173	11.61439	12.58611	11.25	4.7059	0.053079	1.4331	1.553	0.018266	17735.98	20461.3
33.75	43.6079	0.412431	34.85526	19.56729	33.75	7.2158	0.068245	5.7675	3.2378	0.021245	13491.77	20028.47
56.25	55.24059	0.99778	57.84939	18.34562	56.25	6.9686	0.12587	7.2977	2.3143	0.021196	11958.95	20526.49
78.75	36.45064	0.375351	47.8779	37.74315	78.75	3.9764	0.040947	5.223	4.1174	0.026051	13536.85	21409.15
101.25	60.7827	0.196072	73.90453	21.25112	101.25	6.1117	0.019715	7.4311	2.1368	0.027624	20133.56	24845.72
123.75	47.61774	0.737522	47.56975	9.015229	123.75	7.4417	0.11526	7.4342	1.4089	0.020116	24038.18	23651.37
146.25	28.39576	1.083942	20.91924	10.88689	146.25	5.4429	0.20777	4.0098	2.0868	0.009652	15866.95	17429.9
168.75	40.09704	1.795402	25.17194	10.90682	168.75	9.9577	0.44587	6.2512	2.7086	0.011797	9060.664	14736.47
191.25	28.30141	2.803401	31.01916	9.480016	191.25	8.0226	0.79468	8.793	2.6873	0.017146	6441.049	10840.97
213.75	18.11875	4.65094	18.32467	10.67213	213.75	4.5315	1.1632	4.583	2.6691	0.011432	5789.656	10841.78
236.25	13.56817	3.734227	18.37233	13.60804	236.25	3.0968	0.8523	4.1933	3.1059	0.005968	5045.414	9424.734
258.75	5.341766	4.29404	22.60618	8.802238	258.75	1.098	0.88264	4.6467	1.8093	0.006274	5428.457	8290.945
281.25	5.321936	5.940896	22.3109	6.930974	281.25	1.239	1.3831	5.1942	1.6136	0.005343	6268.751	8473.348
303.75	11.08595	2.386442	24.33603	9.906226	303.75	2.4235	0.5217	5.3201	2.1656	0.008721	9768.171	11615.31
326.25	42.58264	4.149046	17.94948	12.99328	326.25	7.9225	0.77193	3.3395	2.4174	0.013617	14585.69	14891.94
348.75	59.50541	3.598518	15.837	11.50881	348.75	5.9434	0.35942	1.5818	1.1495	0.016004	18782.23	19298.75

Appendix B

Percentage Correlation

smcs and strain

	r-value	p
1	0.2941	0.2688
2	**0.6882**	**0.0032**
3	0.3912	0.1341
4	0.3176	0.2306
5	**0.6088**	**0.0123**
6	**0.6529**	**0.0061**

smcs and circss

	r-value	p
1	**0.7529**	**0.0008**
2	0.0706	0.795
3	0.3382	0.2001
4	0.0853	0.7535
5	**0.6794**	**0.0038**
6	0.3206	0.226

smcs and effss

	r-value	p
1	**0.8147**	**0.0001**
2	0.3676	0.1612
3	0.4324	0.0944
4	0.1618	0.5495
5	**0.7029**	**0.0024**
6	**0.6147**	**0.0113**

percentages

1 p3slice1
2 p1slice2
3 p1slice1
4 p1slice3
5 p1slice5
6 p2slice4
7 p2slice1

lip and strain

	r-value	p
1	**0.65**	**0.0064**
2	-0.1324	0.6251
3	0.3	0.2589
4	-0.1147	0.6723
5	**-0.5735**	**0.0202**
6	**0.5676**	**0.0218**

lipid and circss

	r-value	p
1	0.2176	0.4181
2	0.0206	0.9397
3	0.4618	0.0718
4	-0.2235	0.4053
5	**-0.5735**	**0.0202**
6	0.1324	0.6251

lipid and effss

	r-value	p
1	0.4	0.1248
2	0.05	0.8541
3	**0.5412**	**0.0304**
4	-0.1176	0.6643
5	**-0.5618**	**0.0235**
6	0.45	0.0803

mfs and strain

	r-value	p
1	-0.1324	0.6251
2	-0.2088	0.4377
3	**-0.6124**	**0.0117**
4	0.0853	0.7535
5	-0.0794	0.77
6	**-0.8353**	**0.0001**

mfs and circss

	r-value	p
1	**-0.5765**	**0.0194**
2	0.25	0.3504
3	-0.2589	0.333
4	-0.0676	0.8034
5	-0.0559	0.8371
6	**-0.6559**	**0.0058**

mfs and effss

	r-value	p
1	**-0.6059**	**0.0129**
2	0.1029	0.7044
3	-0.3671	0.1619
4	0.0765	0.7783
5	0.0235	0.9311
6	**-0.8647**	**0**

col and strain

	r-value	p
1	-0.3382	0.2001
2	-0.2647	0.3218
3	**-0.8912**	**0**
4	-0.4912	0.0534
5	0.2471	0.3563
6	**0.7941**	**0.0002**

col and circss

	r-value	p
1	-0.2706	0.3108
2	-0.1912	0.4782
3	**-0.6735**	**0.0042**
4	-0.4647	0.0697
5	0.2176	0.4181
6	**0.7706**	**0.0005**

col and effss

	r-value	p
1	-0.3382	0.2001
2	-0.3029	0.2541
3	**-0.7941**	**0.0002**
4	**-0.5294**	**0.035**
5	0.1265	0.6407
6	**0.8324**	**0.0001**

Absolute Correlation

smcs and strain

	r-value	p
1	0.3412	0.1959
2	-0.1912	0.4782
3	**-0.5147**	**0.0413**
4	**-0.5412**	**0.0304**
5	**-0.6882**	**0.0032**
6	0.1618	0.5495

smcs and circss

	r-value	p
1	**0.7882**	**0.0003**
2	-0.4912	0.0534
3	0.1706	0.5276
4	**-0.7912**	**0.0003**
5	**-0.5265**	**0.0362**
6	-0.4412	0.0872

smcs and effss

	r-value	p
1	**0.8647**	**0**
2	-0.4647	0.0697
3	0.0676	0.8034
4	**-0.7382**	**0.0011**
5	**-0.4529**	**0.0781**
6	-0.0912	0.737

absolute

1	p3slice1
2	p1slice2
3	p1slice1
4	p1slice3
5	p1slice5
6	p2slice4

lip and strain

	r-value	p
1	**0.5235**	**0.0374**
2	**-0.6137**	**0.0115**
3	**-0.5324**	**0.0338**
4	-0.415	0.1099
5	**-0.8477**	**0**
6	0.4059	0.1188

lipid and circss

	r-value	p
1	0.0706	0.795
2	-0.443	0.0857
3	0.0588	0.8287
4	**-0.4871**	**0.0557**
5	**-0.7741**	**0.0004**
6	0	1

lipid and effss

	r-value	p
1	0.2147	0.4246
2	**-0.5269**	**0.036**
3	-0.0176	0.9483
4	-0.3959	0.129
5	**-0.7358**	**0.0012**
6	0.2265	0.399

mfs and strain

	r-value	p
1	-0.1676	0.5349
2	**-0.7294**	**0.0013**
3	**-0.6124**	**0.0117**
4	-0.3316	0.2096
5	**-0.9095**	**0**
6	**-0.8559**	**0**

mfs and circss

	r-value	p
1	**-0.6882**	**0.0032**
2	-0.3706	0.1577
3	-0.2589	0.333
4	-0.4318	0.0949
5	**-0.83**	**0.0001**
6	**-0.7853**	**0.0003**

mfs and effss

	r-value	p
1	**-0.7353**	**0.0012**
2	**-0.5647**	**0.0227**
3	-0.3671	0.1619
4	-0.3154	0.2341
5	**-0.7594**	**0.0006**
6	**-0.9324**	**0**

col and strain

	r-value	p
1	-0.3941	0.1309
2	**-0.5382**	**0.0315**
3	**-0.8941**	**0**
4	**-0.6794**	**0.0038**
5	**-0.9353**	**0**
6	**0.5265**	**0.0362**

col and circss

	r-value	p
1	-0.3412	0.1959
2	-0.4824	0.0585
3	**-0.6412**	**0.0074**
4	**-0.5794**	**0.0187**
5	**-0.8441**	**0**
6	0.4088	0.1159

col and effss

	r-value	p
1	-0.4	0.1248
2	**-0.5941**	**0.0152**
3	**-0.7706**	**0.0005**
4	**-0.6647**	**0.005**
5	**-0.8441**	**0**
6	0.4088	0.1159